Published in final edited form as:

Immunity. 2017 September 19; 47(3): 435–449.e8. doi:10.1016/j.immuni.2017.08.012.

Group 1 Innate lymphoid cell lineage identity is determined by a *cis*-regulatory element marked by a long non-coding RNA

Walter K. Mowel[1,2], **Sam J. McCright**[1,2], **Jonathan J. Kotzin**[1,2], **Magalie A. Collet**[3], **Asli Uyar**[3], **Xin Chen**[3,4], **Alexandra DeLaney**[5], **Sean P. Spencer**[1,2], **Anthony T. Virtue**[1,2], **EnJun Yang**[1,2], **Alejandro Villarino**[6], **Makoto Kurachi**[2,7], **Margaret C. Dunagin**[8], **Gretchen Harms Pritchard**[5], **Judith Stein**[9,10], **Cynthia Hughes**[9,10], **Diogo Fonseca-Pereira**[11], **Henrique Veiga-Fernandes**[11,12], **Arjun Raj**[8], **Taku Kambayashi**[1,2], **Igor E. Brodsky**[5], **John J. O'Shea**[6], **E. John Wherry**[2,7], **Loyal A. Goff**[13,14], **John L. Rinn**[15,16], **Adam Williams**[3,17,#], **Richard A. Flavell**[8,9,#], and **Jorge Henao-Mejia**[1,2,18,#]

[1]Department of Pathology and Laboratory Medicine, University of Pennsylvania, Philadelphia, PA 19104, USA

[2]Institute for Immunology, Perelman School of Medicine, University of Pennsylvania, Philadelphia, PA 19104, USA

[3]The Jackson Laboratory for Genomic Medicine, Farmington, CT, 06032, USA

[4]Department of Immunology, University of Connecticut School of Medicine, Farmington, CT, 06030, USA

[5]Department of Pathobiology, School of Veterinary Medicine, University of Pennsylvania, Philadelphia, PA19104, USA

[6]Molecular Immunology and Inflammation Branch, National Institute of Arthritis and Musculoskeletal and Skin Diseases, National Institutes of Health, Bethesda, MD 20892, USA

[7]Department of Microbiology, Perelman School of Medicine, University of Pennsylvania, Philadelphia, PA 19104, USA

Correspondence to: Jorge Henao-Mejia.

[#]Co-corresponding authors

[#]Co-corresponding author contact information:
Adam Williams, adam.williams@jax.org
Richard A. Flavell, richard.flavell@yale.edu
Jorge Henao-Mejia, jhena@mail.med.upenn.edu (lead contact)

Author Contributions

W.K.M., A.W., and J.H.M. designed experiments. J.H.M., R.A.F. and A.W. supervised the project. W.K.M. and J.H.M. wrote the manuscript. A.W. and R.A.F. edited the manuscript. L.A.G. and J.L.R. performed bioinformatics analysis and lncRNA identification. M.A.C., X.C., and A.U. prepared and analyzed ATAC-seq data. M.C.D. and A.R. performed FISH. A.V. and J.J.O. provided STAT5-deficient NK cells and flow cytometry data. J.S. and C.H. aided the generation novel mice. G.H.P. provided the *Tbx21*$^{-/-}$ mice. M.K. generated *Id2* retrovirus. A.D. performed the *Salmonella* infections. All other experiments and analyses were conducted by W.K.M, S.J.M., J.J.K., E.Y., A.T.V., D.F.P., A.W., and J.H.M.

[8]School of Engineering and Applied Science, University of Pennsylvania, Philadelphia, PA 19104, USA

[9]Department of Immunobiology, Yale University School of Medicine, New Haven, CT 06520, USA

[10]Howard Hughes Medical Institute, Yale University, New Haven, CT 06510, USA

[11]Instituto de Medicina Molecular, Faculdade de Medicina de Lisboa, Av. Prof. Egas Moniz, Edifício Egas Moniz, 1649-028 Lisbon, Portugal

[12]Champalimaud Research, Champalimaud Centre for the Unknown, 1400-038 Lisbon, Portugal

[13]McKusick-Nathans Institute of Genetic Medicine, Johns Hopkins University, Baltimore, MD 21205, USA

[14]Department of Neuroscience, Johns Hopkins University, Baltimore, MD 21205, USA

[15]Biological and Biomedical Sciences, Harvard Medical School, Boston, MA 02115, USA

[16]Department of Stem Cell and Regenerative Biology, Harvard University, Cambridge, MA 02138, USA

[17]Department of Genetics and Genomic Sciences, University of Connecticut Health Center, Farmington, CT 06032, USA

[18]Division of Transplant Immunology, Department of Pathology and Laboratory Medicine, Children's Hospital of Philadelphia, University of Pennsylvania, Philadelphia, PA 19104

Summary

Commitment to the innate lymphoid cells (ILC) lineage is determined by *Id2*, a transcriptional regulator that antagonizes T and B cell-specific gene expression programs. Yet how *Id2* expression is regulated in each ILC subset remains poorly understood. We identified a *cis*-regulatory element demarcated by a long non-coding RNA (lncRNA) that controls the function and lineage identity of group 1 ILCs, while being dispensable for early ILC development and homeostasis of ILC2s and ILC3s. The locus encoding this lncRNA, which we termed *Rroid*, directly interacted with the promoter of its neighboring gene, *Id2*, in group 1 ILCs. Moreover, the *Rroid* locus, but not the lncRNA itself, controlled the identity and function of ILC1s by promoting chromatin accessibility and deposition of STAT5 at the promoter of *Id2* in response to interleukin (IL)-15. Thus, non-coding elements responsive to extracellular cues unique to each ILC subset represent a key regulatory layer for controlling the identity and function of ILCs.

Graphical Abstract

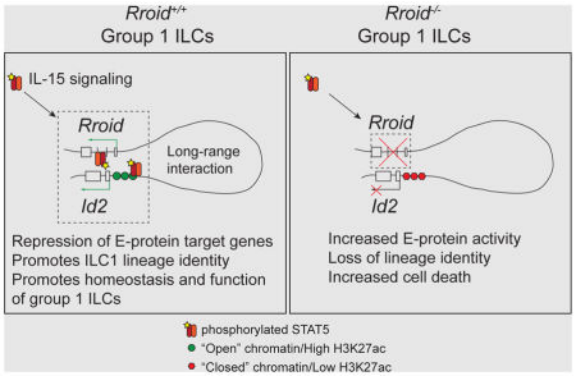

Introduction

Innate lymphoid cells (ILCs) are a recently described class of lymphocytes crucial for the initiation of protective immune responses against viruses, parasites and bacteria. In addition, ILCs integrate tissue-derived and environmental cues to promote metabolic homeostasis and epithelial barrier integrity (Artis and Spits, 2015). Functionally, ILCs are divided into three different groups on the basis of their transcription factor and cytokine expression profiles, in a manner analogous to $CD4^+$ and $CD8^+$ T cell populations (Artis and Spits, 2015). Group 1 ILCs include NK cells and ILC1s, while group 2 and 3 ILCs are comprised of ILC2s and ILC3s, respectively. Although closely related, each ILC subset exhibits unique and distinct epigenetic landscapes that are likely to be essential for their development, function and maintenance of lineage identity (Gury-BenAri et al., 2016; Lara-Astiaso et al., 2014; Shih et al., 2016). Indeed, regions of open and accessible chromatin are known to mark *cis*-regulatory elements such as enhancers, super-enhancers, and long non-coding RNA (lncRNA) promoters that are central to the control of gene expression programs (Engreitz et al., 2016; Fatica and Bozzoni, 2014; Shlyueva et al., 2014). Yet how epigenetic regulatory elements regulate the development, homeostasis and functions of ILCs is largely unknown.

ILCs and adaptive lymphocytes (T and B cells) originate from a common lymphoid progenitor (CLP) in the bone marrow (Zook and Kee, 2016). Commitment and maintenance of the ILC lineage is determined by Inhibitor of DNA Binding 2 (encoded by the gene *Id2*), a transcriptional regulator that antagonizes T and B cell-specific gene expression programs by inhibiting key transcription factors from the E-protein family (Kee, 2009). As such, *Id2* expression is considered a hallmark of ILCs in all species in which these populations have been identified (Zook and Kee, 2016). However, how *Id2* is regulated in ILCs is poorly understood. Given its fundamental role in ILC lineage specification, elucidating the epigenetic mechanisms that control *Id2* expression in each ILC subset is not only critical to understanding the ontogenesis and functions of these innate lymphocyte populations, but may also reveal important clues about their evolutionary origin.

Herein, we report the identification of a *cis*-regulatory element demarcated by the transcription of a lncRNA that is critical for promoting *Id2* expression in group 1 ILCs, but not in ILC2s or ILC3s. We named this lncRNA *Rroid* (**R**NA-demarcated **R**egulatory region **o**f ***Id2***). While the *Rroid* locus was dispensable for early ILC development, it was essential

for determining lineage identity, maturation and function of ILC1s by promoting *Id2*-mediated repression of T and B cell-specific genes. In this ILC subset, the *Rroid* locus, but not the lncRNA itself, was required to promote chromatin accessibility and STAT5 deposition at the *Id2* promoter in response to interleukin (IL)-15, a key cytokine specifically required for the homeostasis of group 1 ILCs. Thus, specific *cis*-regulatory elements demarcated by lncRNAs can determine the function and identity of single ILC subsets. Furthermore, these results indicate that while regulatory elements of *Id2* common to all ILC subsets might control initial commitment to the ILC lineage, epigenetic regulatory elements that are responsive to extracellular cues specific to each group of ILCs are critical to maintaining the identity of individual differentiated ILC subsets.

Results

The long non-coding RNA *Rroid* is expressed in group 1 ILCs

Transcription of lncRNAs is known to mark critical *cis*-regulatory elements, including enhancers and super-enhancers, in a highly cell type-specific manner (Derrien et al., 2012; Engreitz et al., 2016; Shlyueva et al., 2014). In addition, some lncRNAs themselves or the transcription of lncRNA loci have key epigenetic regulatory functions (Carpenter et al., 2013; Engreitz et al., 2016; Kotzin et al., 2016). Because lncRNAs have highly cell type-specific expression patterns, we hypothesized that they might demarcate unique *cis*-regulatory elements that are critical for the function, homeostasis, and/or development of individual ILC subsets, and that these lncRNAs themselves might play key roles in the epigenetic regulation of ILC gene expression programs. To address this hypothesis, we analyzed multiple ATAC-seq and RNA-seq datasets generated from mouse ILC1s, ILC2s and $CD4^+$ ILC3s to identify lncRNAs with two key characteristics: selective expression in single ILC subsets, and located in the vicinity of key genes implicated in ILC development or function (Lara-Astiaso et al., 2014; Shih et al., 2016).

Using this approach, we identified a nuclear transcript (*Ak083360)* that is highly and specifically expressed in ILC1s, but not ILC2s or $CD4^+$ ILC3s (Figure 1A–B), and that exhibits all the features of a lncRNA: *Ak083360* is 2033nt long, not predicted to encode a protein, it has a multi-exon structure, and is spliced and polyadenylated. This lncRNA is located ~220kb upstream of *Id2*, a transcriptional repressor that is a hallmark of all ILC subsets and is essential for their lineage commitment and the maintenance of mature ILC identity (Zook and Kee, 2016). Thus, we named this lncRNA *Rroid* (**R**NA-demarcated **R**egulatory region **o**f **Id**2).

Group 1 ILCs are composed of both “helper” ILC1s and “cytotoxic” ILC1s (NK cells) (Artis and Spits, 2015). To establish whether *Rroid* was also expressed in “cytotoxic” ILC1s (NK cells) and thus restricted to group 1 ILCs, we determined its expression in multiple lymphoid and myeloid populations and whole tissues. Indeed, we found that *Rroid* transcription was preferentially restricted to both cell types that compose group 1 ILCs (NK and ILC1) and to tissues that are highly populated by these cell types (Figure 1C–D). Altogether, these data indicate that the *Rroid* RNA or *cis*-regulatory elements within its locus might have key regulatory functions specifically in group 1 ILCs.

The *Rroid* locus regulates the homeostasis of NK cells and ILC1s, but not ILC2s or ILC3s

To establish the *in vivo* physiological relevance of the *Rroid* locus in the immune system, we used the CRISPR/Cas9 system to generate mice lacking the region encoding *Rroid* (Figure S1A–B). In concordance with the pattern of expression of this lncRNA, mice deficient for the *Rroid* locus (*Rroid*$^{-/-}$) exhibited a dramatic reduction in the frequency and numbers of NK cells (CD3,CD5^{-} NK1.1^{+} NKp46^{+}) in the spleen, liver, and lung (Figure 1E–F). In multiple tissues, NK cells and ILC1s can be distinguished by differential expression of the surface markers CD49a and CD49b or expression of the transcription factors Eomes and T-bet (Klose et al., 2014). *Rroid*$^{-/-}$ mice showed a significant reduction in liver CD49a^{+} ILC1s as well as in T-bet^{+} ILC1s in the lung and intraepithelial lymphocyte (IEL) compartment in the gut (Figure 1G–H). ILC1 populations have also been described in the small intestine lamina propria (SI-LPL) and salivary glands (SG) (Cortez et al., 2016; Klose et al., 2014). However, we found equivalent numbers of SI-LPL and SG ILC1s (Figure 1H), indicating that the *Rroid* locus is not required for the homeostasis of these unique ILC1 populations. Furthermore, intestinal ILC2s and ILC3s, lung ILC2s, and other lymphoid and myeloid population examined at homeostasis were not affected in the absence of *Rroid* (Figure 1I & Figure S1C–F). Taken together, these results indicate that the *Rroid* locus is specifically required for the homeostasis of both ILC1s and NK cells in most tissues, but not ILC2s or ILC3s.

Rroid locus-deficient NK cells are hyporesponsive

We next sought to determine whether the function of group 1 ILCs was altered in response to inflammatory stimuli. In physiological settings, IL-12 synergizes with IL-15 and/or IL-18 to activate a robust IFN-γ response in NK cells and ILC1s (Figure 2A). NK cells can also be activated to degranulate cytotoxic cationic proteins following engagement of activating receptors such as NK1.1 (Figure 2B). However, splenic and liver NK cells from *Rroid*$^{-/-}$ mice exhibited a reduced capacity to produce IFN-γ in response to cytokine stimuli (Figure 2A&C and Figure S2A–B). Likewise, *Rroid*$^{-/-}$ splenic NK cells exhibited reduced expression of Perforin (encoded by *Prf1*) and Granzyme B (GzmB) at steady state, and failed to degranulate efficiently upon crosslinking of NK1.1 (Figure 2B and Figure S2C–E). *Rroid*-deficient liver CD49a^{+} ILC1s did not display a decrease in IFN-γ production upon cytokine stimulation, indicating that in these cells, this regulatory region is dispensable for cytokine production (Figure 2C). To gain insight into the mechanism underlying this difference, we first established the expression of the IL-18 and IL-12 receptors in splenic and liver NK cells. While IL-18 receptor (IL-18R) expression was unaltered (Figure S2F), expression of *Il12rb2,* encoding a component of the IL-12 receptor, was reduced in NK cells from *Rroid*$^{-/-}$ mice as compared to WT mice (Figure 2D and S2G). Activation of the IL-12 receptor induces downstream phosphorylation of STAT4. This process was significantly decreased in *Rroid*-deficient NK cells (Figure S2H). However, in accordance with the absence of a reduction in IFN-γ production in *Rroid*$^{-/-}$ ILC1s, *Il12rb2* expression and p-STAT4 accumulation in liver ILC1s in response to IL-12 stimulation was unaffected (Figure 2D and Figure S2I). These results indicate that the *Rroid* locus is required for NK cell function, in part through regulating responsiveness to IL-12.

We next sought to establish whether the defects observed *ex vivo* had significant physiological consequences. We first determined the capability of *Rroid*-deficient NK cells to clear tumor cells *in vivo* using the RMA tumor cell line system; RMA-S tumor cells are targeted by NK cell due to loss of MHC-I expression (Figure 2E). Indeed, we found that *Rroid*$^{-/-}$ mice were significantly impaired in their ability to clear RMA-S tumor cells (Figure 2E–F). In contrast to the protective effect of NK cells in clearing tumor cells, NK1.1^{+} cells promote bacterial replication during systemic infection with *Listeria monocytogenes* (Lm) (Takada et al., 1994; Viegas et al., 2013). Consistent with these data, *Rroid*$^{-/-}$ mice infected with *Listeria* had significantly reduced bacterial loads in the spleen and liver 3 days post infection (Figure 2G), and *Rroid*$^{-/-}$ NK cell and ILC1 populations in the spleen and liver remained significantly reduced and produced less IFN-γ than their wild-type counterparts (Figure2H–I, **data not shown)**. These results indicate a central role for the *Rroid* locus in regulating the function of NK cells *in vivo* and *ex vivo.*

ILC1s have been shown to provide protection against *Salmonella enterica* serovar Typhimurium (STm) infection (Klose et al., 2013; Spits et al., 2016). Consistent with a lack of defects in SI-LPL ILC1s in *Rroid*-deficient mice, we did not detect significant differences in infection of the Peyer's patches, dissemination to the mesenteric lymph node (MLN) or spleen as well as in the recruitment of myeloid cells 5 days post STm infection (Figure S2J–K, **data not shown)**. Furthermore, *Rroid*$^{-/-}$ NK cells expressed reduced amounts of IFN-γ, whereas IFN-γ production in ILC1s was unchanged (Figure S2L). These results indicate that the *Rroid* locus does not impact ILC1 function in the gut or MLN *in vivo*.

As group 1 ILCs are closely related to ILC2s and ILC3s, and are often functionally regulated by similar pathways, we asked whether ILC2 and ILC3 responses are altered in the absence of the *Rroid* locus. We tested the *in vivo* function of *Rroid*$^{-/-}$ ILC2s using the papain lung inflammation model (Yang et al., 2013). *Rroid*$^{-/-}$ mice treated with papain recruited similar numbers of eosinophils as compared to *Rroid*$^{+/+}$ mice (Figure 2J). Moreover, *Rroid*$^{-/-}$ and wild-type ILC2s expressed equivalent amounts of IL-5 and IL-13 (Figure 2K). These results indicate that *Rroid* is not required for ILC2 responses in the lung. In the gut, ILC3s mediate multiple processes; including the induction of Peyer's patch organogenesis by the ILC3 subset lymphoid tissue inducer (LTi) cells. *Rroid*$^{-/-}$ mice exhibited normal numbers of Peyer's patches, indicating that LTi cells function normally in the absence of the *Rroid* locus (Figure 2L). In inflammatory settings, the cytokines IL-23 and IL-1β activate ILC3s to secrete IL-22. IL-22 production was unchanged in *Rroid*$^{-/-}$ ILC3s, indicating that *Rroid* does not regulate cytokine production in ILC3s (Figure 2M). Finally, as IFN-γ production is regulated similarly in group 1 ILCs, CD4^{+} T cells and CD8^{+} T cells, we examined the production of this cytokine in these adaptive lymphocytes. We found that production of IFN-γ was unaltered in *in vitro* polarized CD4^{+} Th1 cells and activated CD8^{+} T cells from *Rroid*$^{-/-}$ mice (Figure S2M–O), indicating that the *Rroid* locus is dispensable for cytokine responses in activated T cells. Taken together, our results indicate that the *Rroid* locus is specifically required for the homeostasis and function of group 1 ILCs, but not ILC2s or ILC3s.

The *Rroid* locus is required for the maturation of NK cells

Because the *Rroid* locus controls the frequency and function of group 1 ILCs, we next sought to examine whether it is necessary for initial commitment to the NK cell and ILC1 lineages, their development, or maturation. Using *Rroid* RNA expression as a proxy for activity at this locus, we found that *Rroid* was not expressed in bone marrow lymphoid-primed multipotent progenitor (LMPP) cells or CLPs, which give rise to both ILCs and adaptive lymphocytes (Figure 3A). We also failed to find differences in the numbers of bone marrow LMPPs, CLPs, or common helper ILC progenitors (CHILPs) in the absence of the *Rroid* locus (Figure 3B–C). NK cells are traditionally thought to develop from pre-NK cell progenitors (pNKP) and refined-NKP (rNKP), identified by defined cell surface markers (Figure S3A) (Fathman et al., 2011). In addition to NKPs, these populations also contain small numbers of cells marked by expression of *Zbtb16* (also called PLZF), that are progenitors of helper ILCs, including ILC1s (Constantinides et al., 2015; Constantinides et al., 2014). We did not observe any defects in NK cell (pNKP, rNKP) or ILC ($PLZF^+$ pNKP/rNKP) progenitors in $Rroid^{-/-}$ mice (Figure 3B&D). Finally, the bone marrow NK cells and ILC1 populations were also unaffected (Figure 3E). Altogether, these results indicate that the *Rroid* locus is not required for group 1 ILC lineage commitment or their early development.

We then assessed the processes regulated by the *Rroid* locus in peripheral group 1 ILC populations. Following the production of new NK cells in the bone marrow, immature NK cells undergo a maturation process driven by the cytokine IL-15, which is characterized by the acquisition of the surface marker CD11b, loss of CD27, and increased proliferation and survival (Figure 3F) (Chiossone et al., 2009; Polansky et al., 2016). Ablation of the *Rroid* locus resulted in a block of NK cell maturation characterized by accumulation of immature $CD27^+$ NK cells and a near complete loss of mature $CD11b^+$ NK cells (Figure 3F–G). This block in maturation was accompanied by impairment in the proliferation and survival capacity of maturing $Rroid^{-/-}$ NK cells as determined by BrdU incorporation and Annexin V staining (Figure 3H). As IL-15 is essential for the maturation of group 1 ILCs, we next sought to establish whether signaling through the IL-15 receptor was altered in NK cells in the absence of the *Rroid* locus. Although CD122 (a component of the IL-15 receptor) was expressed at significantly higher levels in $Rroid^{-/-}$ NK cells, phosphorylation of STAT5 was unaltered in the absence of the *Rroid* locus (Figure S3B–C), indicating that IL-15 receptor signaling is intact in $Rroid^{-/-}$ mice. Finally, using mixed bone marrow chimeras we found that *Rroid*-deficient NK cells retained significant defects in maturation and cytokine production, indicating that the *Rroid* locus controls NK cell function and maturation in a cell-intrinsic manner (Figure 3I and Figure S3D). Altogether, these data indicate that the *Rroid* locus regulates group 1 ILC populations by promoting their maturation, proliferation, and survival.

The *Rroid* locus promotes *Id2* expression to control group 1 ILC homeostasis

Our findings reveal a critical role for the *Rroid* locus in the homeostasis, maturation, and function of group 1 ILCs. *Cis*-regulatory elements and lncRNAs can control the expression of neighboring genes (Engreitz et al., 2016; Kotzin et al., 2016; Lam et al., 2014; Rinn and Chang, 2012), but lncRNAs are also known to act in *trans* to regulate gene expression

programs (Carpenter et al., 2013). Therefore, to identify the regulatory functions of the *Rroid* locus in group 1 ILCs through an unbiased approach that accounts for both possibilities, we performed RNA-seq on sort-purified splenic DP ($CD27^+$ $CD11b^+$) NK cells. Among 58 significantly differentially expressed transcripts, the canonical ILC gene, *Id2*, was reduced in these cells (Figure 4A, Table S1). Similarly, splenic and liver NK cells as well as liver ILC1s from $Rroid^{-/-}$ mice showed significantly decreased levels of *Id2*, while key transcription factors required for their normal development (*Ets1, Tox, Nfil3, T-bet*, and *Eomes*) were unaltered (Figure 4A–C and Figure S4A–B). In accordance with *Rroid*'s pattern of expression and the lack of defects in the frequency and function of ILC2 and ILC3 populations in *Rroid*-deficient mice, *Id2* expression was not dysregulated in sorted small intestine ILC3s or IL-33 elicited lung ILC2s from $Rroid^{-/-}$ animals, nor it was altered in *in vitro* polarized Th1 cells or activated $CD8^+$ T cells (Figure 4D and Figure S4C). These results indicate that the *Rroid* locus is promotes *Id2* expression specifically in peripheral group 1 ILCs.

Id2 expression is required for commitment to the ILC lineage during early development in the BM and maintains the identity of mature ILCs by directly antagonizing E-protein transcription factors, which are critical for promoting T and B cell lineage-specific gene expression programs (Kee, 2009; Zook and Kee, 2016). Therefore, we sought to establish whether *Rroid*-mediated regulation of *Id2* in group 1 ILCs is required to prevent the aberrant expression of genes classically associated with adaptive lymphocytes in group 1 ILCs. Gene set enrichment analysis (GSEA) confirmed a significant enrichment of known *Id2*-dependent genes in our RNA-seq dataset (Figure 4E)(Delconte et al., 2016). Furthermore, expression of T and B cell specific genes (e.g. *Cd3d*, *CD3g*) was significantly increased in NK cells deficient for the *Rroid* locus (Figure 4A&F). These data imply that E-protein mediated transcriptional activation of adaptive lymphocyte genes is increased in $Rroid^{-/-}$ NK cells. To address this possibility, we mapped genome-wide open chromatin using ATAC-seq and performed transcription factor footprinting analysis to determine whether canonical E-protein binding sites were enriched in $Rroid^{-/-}$ NK cells. Transcription factor footprinting analysis revealed enrichment of binding sites for E2A and E2-2 (encoded by *Tcf3* and *Tcf4*, respectively) within the 2837 open chromatin peaks specific to *Rroid*-deficient NK cells (Figure 4G–H). Furthermore, both binding sites and expression of the E-protein target *Tcf7* (Delconte et al., 2016; Masson et al., 2013) were also enriched in regions of open chromatin specific to $Rroid^{-/-}$ NK cells (Figure 4H and Figure S4D). Consistent with our previous finding indicating that adaptive lymphocyte genes are derepressed in the absence of the *Rroid* locus, open chromatin peaks in $Rroid^{-/-}$ NK cells were significantly associated with genes in the T and B cell receptor signaling pathways (Figure 4I). Together, these results suggest that the *Rroid* locus maintains group 1 ILC lineage identity by promoting *Id2*-mediated repression of E-protein target genes.

Finally, to formally determine whether downregulation of *Id2* in *Rroid*-deficient group 1 ILCs is the key alteration impairing their identity, maturation, and function, we reconstituted lethally irradiated hosts with $Rroid^{-/-}$ bone marrow transduced with a retrovirus encoding *Id2* (Figure 4J). Restoring *Id2* expression in $Rroid^{-/-}$ bone marrow cells resulted in increased peripheral NK cell populations and a reversal of their maturation defects (Figure

4J–L). Altogether, these data indicate that the *Rroid* locus promotes peripheral group 1 ILC homeostasis and maturation primarily through its role in regulating *Id2* expression.

The *Rroid* locus controls open chromatin and recruitment of STAT5 to the *Id2* promoter

Both *cis*-regulatory elements and lncRNAs can regulate gene expression through epigenetic mechanisms such as controlling chromatin accessibility and histone modifications at the promoters of their target genes (Rinn and Chang, 2012). To determine whether the *Rroid* locus regulates *Id2* expression in group 1 ILCs through epigenetic mechanisms, we performed ChIP-qPCR for histone modifications at the *Id2* promoter in NK cells and analyzed the *Id2* locus in our ATAC-seq dataset. In the absence of the *Rroid* locus, histone marks associated with active promoters (H3K27ac) and transcription (H3K36me3) were significantly decreased at the *Id2* promoter and gene body, respectively (Figure 5A). In accordance with these data, analysis of our ATAC-seq results also revealed decreased chromatin accessibility within the *Id2* promoter in $Rroid^{-/-}$ NK cells, while gene expression and chromatin accessibility of genes within 1MB up- and downstream of *Id2* were unaltered (Figure 5B–E & S5A–B). Together, these results indicate that proper chromatin accessibility and activating histone modification levels at the *Id2* promoter in NK cells require the *Rroid* locus.

Among all ILCs, both NK cells and ILC1s are unique in that they require IL-15 for their maturation, function, and homeostasis (Klose et al., 2014). Furthermore, IL-15 has been previously shown to induce *Id2* expression in NK cells (Delconte et al., 2016). Thus, we next investigated whether the *Rroid* locus is required for IL-15-mediated control of *Id2* in group 1 ILCs. Using *Rroid* transcription as a proxy for activity at the *Rroid* locus, we found that IL-15 induced both *Id2* and *Rroid* expression in NK cells in a dose-dependent manner (Figure 5F). Moreover, IL-15 mediated induction of *Id2* expression was dependent on the *Rroid* locus (Figure 5G). Engagement of the IL-15 receptor directly activates downstream STAT5 signaling in group 1 ILCs (Figure S3C). Thus, we next sought to establish whether STAT5 regulates *Id2* expression through the *Rroid* locus. Using STAT5-deficient mice expressing only a single allele of *Stat5b* (*$Stat5a^{-/-}$ $Stat5b^{+/-}$),* we observed that STAT5 was required for NK cell maturation as well as induction of *Id2* transcription in NK cells *in vivo* (Figure 5H–I). Additionally, in the absence of the *Rroid* locus, STAT5 occupancy was significantly decreased at the *Id2* promoter (Figure 5J). While the transcription factor T-bet (encoded by *Tbx21*) is known to be essential for the homeostasis of both NK cells and ILC1s, we did not find a role for T-bet in the regulation of *Id2* (Figure S5C–G). Altogether, these results indicate that the *Rroid* locus is required for adequate STAT5 deposition at the *Id2* promoter in ILC1s*,* and thus critical for IL-15-mediated regulation of *Id2* expression.

An ILC1-specific subdomain within the *Rroid* locus regulates NK cells

Our results indicate a critical role for the *Rroid* locus in promoting group 1 ILC homeostasis through its regulation of *Id2*. Transcription of lncRNAs is known to mark important regulatory regions, but can also directly control gene expression (Derrien et al., 2012; Engreitz et al., 2016; Kotzin et al., 2016; Rinn and Chang, 2012). Thus, to determine whether DNA elements within the *Rroid* locus or the lncRNA itself regulate *Id2* expression in NK cells, we first utilized locked nucleic acids (LNAs) to decrease the levels of *Rroid* in

cultured NK cells *in vitro* (Figure 6A). Using this system, we observed a significant depletion of *Rroid* RNA in wild-type NK cells electroporated with LNAs targeting *Rroid* (Figure 6B). However, acute depletion of *Rroid* in mature NK cells *ex vivo* did not result in significant changes in *Id2* expression levels during the culture period (Figure 6B), indicating that the *Rroid* lncRNA might not be required for the maintenance of *Id2* expression in mature NK cells.

We next asked whether specific open chromatin sites within the *Rroid* locus unique to ILC1 are required for *Id2* expression or for the homeostasis and maturation of these cells. Using ATAC-seq datasets for the different ILC populations, we identified two elements within the *Rroid* locus that are uniquely open and accessible in ILC1s, which are specifically localized in the promoter region and second intron of the *Rroid* lncRNA locus (Figure 6C). Using chromatin conformation capture (3C), ChIP-seq data, and ChIP-qPCR, we found that these ILC1-specific sites located within the *Rroid* locus formed a long-range interaction with the *Id2* promoter, and were bound by STAT5 upon IL-15 stimulation (Figure 6D–E and Figure S6A). Thus, to establish the role of these ILC1-specific open chromatin sites, we generated mice lacking the promoter region and first exon of *Rroid* (*Rroid-P1*) or the putative regulatory element in *Rroid*'s second intron (*Rroid-RE1;* Figure S6A–D). We did not observe a reduction in *Rroid* levels in either of these two new mouse strains (Figure 6F), indicating that that *Rroid* has alternative transcriptional start sites (TSS). Deletion of *Rroid-P1* did not affect NK cell maturation or *Id2* expression (Figure 6G–J). However, *Rroid-RE1*$^{-/-}$ mice have a significantly lower proportion of mature NK cells and a reduction in *Id2* levels in these cells (Figure 6G–J), partially recapitulating the phenotype observed in *Rroid*$^{-/-}$ mice. This indicates that while the RE1 *cis*-regulatory element contributes to the regulation of *Id2*, it is likely that additional regulatory elements within the *Rroid* locus, or potentially transcription across *Rroid* locus, are required for appropriate control of *Id2* expression in group 1 ILCs *in vivo*.

Discussion

In this study, we showed that a *cis*-regulatory element demarcated by the transcription of the lncRNA *Rroid* regulates the maturation, function, and lineage identity of group 1 ILCs, but not of ILC2s or ILC3s. Furthermore, we showed that in response to the cytokine IL-15, the *Rroid* locus regulates the functions and lineage identity of ILC1s by promoting chromatin accessibility and STAT5 deposition at the promoter of the ILC-lineage defining factor Id2, providing evidence that non-coding elements responsive to extracellular cues unique to each ILC subset are critical to control the identity and function of ILCs.

LncRNAs regulate gene expression programs through direct and indirect mechanisms (Derrien et al., 2012; Engreitz et al., 2016; Kotzin et al., 2016; Rinn and Chang, 2012). Several described lncRNAs directly interact with chromatin modifying complexes or transcription factors to modulate gene expression (Rinn and Chang, 2012). Furthermore, transcription across lncRNA loci, but not the RNA molecules, has been shown to be required for proper expression of neighboring genes (Engreitz et al., 2016). While the molecular mechanisms by which transcription of lncRNAs regulate gene expression in *cis* are not fully elucidated, recent evidence indicates that this process is required to promote chromatin

accessibility, epigenetic modifications or to regulate transcriptional initiation of target genes (Anderson et al., 2016; Engreitz et al., 2016). We showed that acute depletion of the *Rroid* RNA in mature NK cells *ex vivo* did not impact *Id2* levels, suggesting that the *Rroid* lncRNA itself does not directly regulate *Id2* expression. Furthermore, we attempted to ablate *Rroid* transcription by deleting the putative *Rroid* promoter (*Rroid-P1*), yet we did not observe a reduction in *Rroid* transcript levels in *Rroid-P1*$^{-/-}$ NK cells, indicating that this lncRNA contains alternative downstream promoters. While these results precluded us from addressing the role of transcription along the *Rroid* locus in the regulation of *Id2* expression, the *Id2-Rroid* regulatory axis described here represents a highly physiologically-relevant system with a clear *in vivo* function that could be used to dissect the role of transcription across lncRNAs in gene expression regulation in the future.

Long-range chromatin looping interactions between promoters and enhancers play a critical role in the regulation of gene expression (Bulger and Groudine, 2011). Chromatin loops in mammalian genomes are determined by cohesin and CTCF. Cohesin promotes the extrusion of chromatin loops until it encounters CTCF bound to DNA (Merkenschlager and Nora, 2016). While CTCF binds specific DNA sequences, recent evidence indicates that transcription significantly contributes to positioning cohesin in the mammalian genome (Busslinger et al., 2017). Here we showed that the *Rroid* locus and *Id2* promoter interact with each other through a long-range chromatin loop. Moreover, we showed that transcription of *Rroid* positively correlates with *Id2* levels in mature group 1 ILCs. It will be important in future studies to establish the role of *Rroid* transcription in the localization of CTCF and cohesin at this locus, and in the formation of this long-range chromatin interaction. Moreover, it will be critical to determine at which point during the development or maturation of ILC1 this long-range interaction is formed and whether a similar three-dimensional architecture is found in ILC2s and ILC3s.

Early commitment to the ILC lineage requires the repression of T and B cell gene expression programs by the transcriptional regulator *Id2* (Zook and Kee, 2016). Moreover, tightly regulated *Id2* expression maintains the lineage identity of differentiated ILCs and thus it is critical for their function (Delconte et al., 2016). Yet how *Id2* expression is regulated in mature ILCs has remained largely unknown. In this study, we showed that the regulatory element demarcated by the lncRNA *Rroid* is key for promoting *Id2* expression in mature group 1 ILCs, but is dispensable for *Id2* transcription during early ILC development or in differentiated ILC2s and ILC3s. These results suggest that commitment of hematopoietic precursors to the ILC lineage and the maintenance of lineage identity in each mature ILC population is differentially controlled by specific epigenetic regulatory elements at the *Id2* locus. Thus, identification of highly conserved elements required for *Id2* transcription during early commitment to the ILC lineage could reveal important clues about the early development and evolutionary origin of these cells (Vivier et al., 2016). Finally, our results suggest that the functional characterization of ILC subset-specific epigenetic regulatory elements or lncRNAs at the *Id2* locus will be critical for understanding how the maturation, homeostasis and effector functions of each ILC subset are controlled in the periphery.

One important factor influencing the epigenetic state of immune cell populations are extracellular signals derived from the tissue microenvironment. Indeed, the homeostasis and

function of the different ILC subsets is controlled by well-characterized tissue- and environmental-derived cues (Zook and Kee, 2016). For example, NK cells and ILC1s are unique in that they require IL-15 for their differentiation, function and homeostasis (Klose et al., 2014). Recent evidence suggests that IL-15 regulates group 1 ILCs by promoting *Id2* expression (Delconte et al., 2016). In this study, we found that STAT5 binds to specific elements within the *Rroid* locus in response to IL-15 stimulation in NK cells and that this locus is necessary for adequate STAT5 deposition at the *Id2* promoter in ILC1s, which in turn is critical to induce *Id2* expression. Thus, our results provide key mechanistic insight on how IL-15 regulates ILC1 functions and lineage identity. In ILC2s and ILC3s, signaling through the IL-2 and IL-7 receptors also activates STAT5 and regulates the homeostasis and function of these cells (Eberl et al., 2004; Moro et al., 2010). However, the *Rroid* locus was dispensable for *Id2* expression in ILC2s and ILC3s. These results suggest that *cis*-regulatory elements, and potentially lncRNAs, that are specific for ILC2s and ILC3s may be required for the binding of STAT5 or other key transcription factors at the *Id2* locus to specifically induce its expression in these cell-types. More broadly, our results suggest that identifying and functionally characterizing other key epigenetic regulatory elements within the *Id2* locus will be an important step for understanding the development and function of mature tissue-resident ILC populations and their precursors.

In summary, our results provide the first evidence that a *cis*-regulatory element demarcated by a lncRNA is critical for the function, homeostasis and lineage identity of a specific ILC subset. Moreover, this work indicates that epigenetic elements unique to each ILC subset represent a crucial regulatory layer that determines ILC lineage identity and functional specification.

STAR Methods

CONTACT FOR REAGENT AND RESOURCE SHARING

Further information and requests for resources and reagents should be directed to and will be fulfilled by the Lead Contact, Jorge Henao-Mejia (jhena@mail.med.upenn.edu).

EXPERIMENTAL MODEL AND SUBJECT DETAILS

Mice—C57BL/6 (*Rroid*$^{+/+}$), B6.SJL-*Ptprc*^{a} *Pepc*^{b}/Boy (CD45.1^{+}), and B6(SJL)-*Zbtb16*$^{tm1.1(EGFP/cre)Aben}$ (PLZF^{GFPcre}) mice were purchased from The Jackson Laboratory. Generation of STAT5-deficient mice (*Stat5a*$^{-/-}$ *Stat5b*$^{+/-}$) was described previously (Villarino et al., 2016). The *Tbx21*$^{-/-}$ mice were from Christopher Hunter. The *Rroid*$^{-/-}$, *Rroid-P1*$^{-/-}$, *and Rroid-RE1*$^{-/-}$ mice were generated using the CRISPR/Cas9 system as described (Henao-Mejia et al., 2016). Briefly, we designed sgRNAs flanking the loci of interest and used these sgRNAs and Cas9 to generate double-stranded DNA breaks in C57BL/6 single cell embryos, which were resolved by non-homologous end joining, ablating the intervening sequence. The sgRNA sequences and targeting schema are found in Figures S1, S6, and in the Key Resources Table. Genomic deletion of the *Rroid* locus was confirmed by PCR. One *Rroid*$^{+/-}$ line was established and backcrossed onto the C57BL/6 background for at least 5 generations to control for potential off-target effects, then intercrossed to generate *Rroid*$^{-/-}$ mice. For *Rroid-P1* and *Rroid-RE1*-deficient mice,

genomic deletions in founder mice were confirmed by PCR and bred by crossing heterozygotes with either heterozygous or homozygous mates; in these experiments, littermate *Rroid*$^{+/+}$ controls were used. All mice were bred and maintained under pathogen-free conditions at an American Association for the Accreditation of Laboratory Animal Care accredited animal facility at the University of Pennsylvania or National Institutes of Health. Mice were housed in accordance with the procedures outlined in the Guide for the Care and Use of Laboratory Animals under an animal study proposal approved by an institutional Animal Care and Use Committee. Male and female mice between 6 and 12 weeks of age were used in this study.

Bacteria—Single *Listeria monocytogenes* 1043S colonies were picked from Brain Heart Infusion (BHI) agar and cultured in BHI broth shaking at 250rpm at 37°C. Single *Salmonella enterica* serovar Typhimurium (strain SL1344) colonies were picked from LB plates and grown in LB broth shaking at 250rpm at 37°C.

METHOD DETAILS

Cell isolation—Single cell suspensions from mouse spleen and mesenteric lymph node were isolated by physical dissociation and filtered through a 70μm cell strainer. For bone marrow cell isolation, femurs were collected and flushed with 5mL of cold PBS, then filtered with a cell strainer. For sorts, bone marrow was collected from femurs and tibias by crushing using a mortar and pestle.

For lungs, mice were perfused with 10mL of PBS through the right ventricle of the heart prior to isolation. The lungs were then isolated, minced with scissors, and digested in RPMI + 1mg/mL Collagenase D + 0.2mg/mL DNase I for 45 minutes at 37°C with shaking at 200rpm. The digested lungs were then passed through a 70μm cell strainer. The cells were pelleted and purified by bringing up in 40% isotonic Percoll, underlaying 80% isotonic Percoll, and spinning at 800xg for 20min at 4°C with low brake. Hematopoietic cells were collected from the interface.

For isolation of murine liver leukocytes, the liver was perfused with 10ml PBS and then transferred to DMEM on ice. The liver was then removed from media and minced into small pieces prior to digestion with DMEM+ 0.5mg/mL Collagenase 4 + 0.2mg/mL DNase I for 45min at 37°C with shaking at 200rpm. The digested livers were then passed through a 100μm cell strainer; the remaining pieces were mashed through the same strainer. To pellet hepatocytes, the digested livers were centrifuged at 20xg for 5min at 4°C. The leukocyte-containing supernatant was then transferred to a new tube and centrifuged at 450xg for 5min at 37°C. The collected leukocytes were purified over a Percoll gradient as described for lung leukocyte isolation.

For isolation of small intestine lamina propria lymphocytes, the small intestine was obtained, opened lengthwise, and the feces shaken out by agitation in ice cold PBS. Mucus and epithelial cells were removed by first incubating 2×15min at 180rpm and 37°C in HBSS (Corning) + 2%FBS (Sigma)+ 20mM HEPES (ThermoFisher Scientific)+ 5mM DTT (Sigma), then 2×15min at 180rpm and 37°C in HBSS+ 2%FBS+ 20mM HEPES+ 5mM EDTA, pH8.0. Intestines were thoroughly washed 2x with ice cold PBS and minced into

small pieces with scissors. The minced small intestines were then digested in 20mL RPMI (Corning)+ 20mM HEPES+ 1X Penicillin/Streptomycin (ThermoFisher Scientific) + 0.05mg/mL Liberase TM+ 0.2mg/mL DNase I. The digested intestines were filtered through a 100μm cell strainer and purified over a Percoll gradient.

For isolation of intestinal epithelial lymphocytes, the small intestine was obtained and opened lengthwise as above. Mucus was removed by incubating 2×15min at 180rpm and 37°C in HBSS+ 2%FBS+ 20mM HEPES+ 5mM DTT. The intestines were then incubated 2×15min at 180rpm and 37°C in HBSS+ 2%FBS+ 20mM HEPES+ 5mM EDTA, pH8.0. The washes were filtered through a 70μm cell strainer, pelleted, and lymphocytes were purified over a Percoll gradient as above.

For isolation of salivary gland lymphocytes, salivary glands were obtained and minced in digest medium containing RPMI + 20mM HEPES + 1mg/mL Collagenase D + 0.2mg/mL DNase I for 45 minutes at 37°C with shaking at 180rpm. The digested salivary glands were filtered and mashed through a 70μm cell strainer. The cells were pelleted and purified over a Percoll gradient as above.

For all tissues preparations, red blood cells were lysed using ACK lysing buffer (ThermoFisher Scientific) for 5 minutes on ice, pelleted, and brought up in FACS buffer (PBS+ 2%FBS+ 1mM EDTA).

Antibodies, Flow cytometry, and cell sorting—Antibodies listed in the Key Resources Table were diluted in FACS buffer (PBS + 2%FBS + 2mM EDTA) and used to stain single cell suspensions for 20 minutes in the dark at 4°C. Cells were washed with FACS buffer and either fixed for intracellular staining or subjected to flow cytometry. Dead cells were eliminated with DAPI, 7-AAD, or Live/Dead Aqua.

For sorts, cells were sorted according to the following scheme: NK cells ($CD3e^-$ $NK1.1^+$ $NKp46^+$ or $CD3e^-$ $NK1.1^+$ $CD49b^+$), CD4 T cells ($CD19^-$ $CD3^+$ $CD4^+$), CD8 T cells ($CD19^-$ $CD3^+$ $CD8^+$), B cells ($CD3^-$ $CD19^+$), macrophages ($F4/80^+$ $CD11b^+$), liver NK cells ($CD3e^-$ $NK1.1^+$ $NKp46^+$ $CD49a^-$ $CD49b^+$), liver ILC1 ($CD3e^-$ $NK1.1^+$ $NKp46^+$ $CD49a^+$ $CD49b^-$), small intestine ILC2 (Lin^- $CD45.2^+$ $CD90.2^+$ $CD127^+$ $KLRG1^+$), small intestine ILC3 (Lin^- $CD45.2^+$ $CD90.2^+$ $CD127^+$ $KLRG1^-$), lung ILC2 (Lin^- $CD45.2^+$ $CD90.2^+$ $T1/ST2^+$). The gating strategy for sorting CLP and NK cell progenitors is depicted in Figure S3A. Lineage (Lin) markers included CD3, CD4, CD8, CD11b, CD11c, Ly6G, NK1.1, and Ter119.

To sort NK cells for culture, up to 5 spleens were pooled, stained with a lineage antibody cocktail against CD3, CD4, CD8, CD19, and Ter119; these cells were depleted with Anti-Rat IgG magnetic beads (Qiagen). Cells were subsequently stained with antibodies to NK1.1 and NKp46 or CD49b. Live cells were sorted as $DAPI^-$ Lin^- $NK1.1^+$ $NKp46^+$ or $DAPI^-$ Lin^- $NK1.1^+$ $CD49b^+$. Cell sorting was performed on a FACS Aria II (BD Biosciences). Flow cytometry was performed on a LSR-II (BD Biosciences). Transcription factor staining was done using the FoxP3 Transcription Factor Staining Kit (ThermoFisher Scientific) according to the manufacturer's instructions. Incorporation of BrdU was detected using the

BrdU staining buffer set (ThermoFisher Scientific) according to the manufacturer's instructions.

Intracellular cytokine staining—Leukocytes isolated from spleen, liver, lung parenchyma, and small intestine lamina propria were plated in 96-well round bottom plates in DMEM+ 5% FBS+ 20mM HEPES+ and 1X Penicillin/Streptomycin and held at 37°C. Media containing the indicated cytokines (final concentration 20ng/mL) or PMA (Sigma; final concentration 100ng/mL) and Ionomycin (Sigma; final concentration 10ng/mL) was then added to the appropriate wells. Cytokine secretion was blocked with Brefeldin A (Sigma). The cell suspensions were stimulated for 4–5h at 37°C. For intracellular cytokine detection, cells were washed and fixed with Cytofix/cytoperm (BD Biosciences) or Foxp3 Transcription Factor Staining Kit and permeabilized with Permeabilization Buffer (ThermoFisher Scientific) according to the manufacturer's instructions.

RNA fluorescence *in situ* hybridization—Single molecule RNA fluorescence *in situ* hybridization (FISH) was performed as previously described (Kotzin et al., 2016). Briefly, sorted B and NK cells from C57BL/6 wild-type mice were fixed and stained with a pool of 24 oligonucleotides (Biosearch Technologies) labeled with Cy3 (GE Healthcare). For validation purposes, we also labeled subsets consisting of odd and even numbered oligonucleotides with Cy3 and Alexa 594 (ThermoFisher Scientific), respectively, and looked for colocalization of signal. We designed the oligonucleotides using the online Stellaris probe design software (https://www.biosearchtech.com/support/tools/design-software/stellaris-probe-designer). Twenty *Z*-sections with a 0.3-μm spacing were taken for each field of view. We acquired all images using a Nikon Ti-E widefield microscope with a 100× 1.4NA objective and a Pixis 1024BR cooled CCD camera.

BrdU Labeling—For BrdU labeling experiments, mice were injected with 1mg Bromodeoxyuridine (Sigma) in 200uL PBS every 12h for three days and sacrificed for analysis 12hr after the final administration.

***In vivo* RMA challenge—**Prior to the experiment, RMA cells were labeled with CFSE (ThermoFisher Scientific) and RMA-S were labeled with Cell Trace Violet (CTV; ThermoFisher Scientific) according to the manufacturer's instructions. 5×10^6 CFSE-labeled RMA cells (MHC-I$^+$) and 15×10^6 CTV-labeled RMA-S (MHC-I$^-$) cells were combined in 200uL of PBS in injected intravenously into recipients. After 16h, the recipient mice were euthanized and splenocytes were analyzed by flow cytometry. The results were determined by taking the ratio of RMA:RMA-S cells remaining in the spleen at this time.

***Listeria monocytogenes* and *Salmonella* Typhimurium infections—**For *Listeria* infections, mice were injected i.v. with 3×10^4 CFU of *Listeria monocytogenes* 1043S. The mice were sacrificed 3 days post infection and their spleens and livers were collected for flow cytometry and CFU analysis. For *Salmonella* infections, mice were fasted 12 hours prior to oral gavage with 5–7×10^7 CFU of *Salmonella enterica* serovar Typhimurium (strain SL1344). Food was returned to mice immediately post infection. Mice were sacrificed day 5 post infection and their organs were collected and homogenized for flow cytometry and CFU analysis.

Papain challenge—Papain challenge was done by anesthetizing mice with Isoflurane and administering 30μg of Papain in 30μL PBS every 24 hours for five days. Mice were sacrificed for analysis 24hr after the last challenge.

Intranasal IL-33—To elicit lung ILC2 expansion, we intranasally administered recombinant murine IL-33 (Biolegend). Mice were anesthetized with Isoflurane and treated with 250ng IL-33 diluted in 25μL PBS every 24 hours for 4 days. Mice were sacrificed for sorting 24 hours after the last administration.

***In vivo* IL-2/αIL-2 treatment—**To generate IL-2/αIL-2 complexes for the *in vivo* expansion of mouse NK cells, we incubated 1.5μg recombinant murine IL-2 (Peprotech) with 10μg αIL-2 (S4B6; BioXcell) in 50uL sterile PBS at 37°C for 30 minutes. The complexes were then diluted to 200μL in PBS and injected i.p. into mice every other day for a total of three administrations. Mice were sacrificed 24 hours following the final administration.

Bone marrow chimeras—To generate competitive bone marrow chimeras, bone marrow from either *Rroid*$^{+/+}$ CD45.1^{+}CD45.2^{+} or *Rroid*$^{-/-}$ (CD45.2^{+}) donor mice was isolated by flushing. Following red blood cell lysis, donor cells were counted and mixed 1:1. A total of 1×10^{6} donor bone marrow cells were transferred intravenously into lethally irradiated (2×550rad given 3h apart) CD45.1^{+} hosts. Recipients were maintained on water supplemented with Sulfatrim for two weeks following the transfer. Mice were sacrificed for analysis 8 weeks following transfer.

Retroviral transduction—Retrovirus for transducing *Rroid*$^{-/-}$ bone marrow was generated as previously described (Kurachi et al., 2014). Briefly, *Id2* cDNA was cloned into the MSCV-IRES-GFP plasmid. Empty or Id2-expressing retrovirus were produced in 293T human embryonic kidney cells with MSCV expression and pCL-Eco packaging plasmids using Lipofectamine 3000 (Invitrogen) according to the manufacturer's instructions.

Bone marrow for transduction was isolated by flushing femurs and tibias from *Rroid*$^{-/-}$ mice 4 days after treatment with 5mg 5-Fluorouracil. Bone marrow cells were seeded at 2.5×10^{6} cells/mL in a 6-well plate in IMDM+ 15% FBS+ 1X Penicillin/Streptomycin+ 10ng/mL IL-3+ 5ng/mL IL-6+ and 100ng/mL SCF (Biolegend) and cultured overnight. Cultures were readjusted to 5×10^{6} cells/mL in 1mL culture medium, and 1mL of retroviral supernatants supplemented with 10μg/mL Prolybrene (EMD Millipore) was added to the appropriate wells. Cells were spinfected at 230xg for 2h at room temperature, then incubated at 37°C overnight. Transduced bone marrow was then washed and transferred to lethally irradiated hosts. The day before transfer, CD45.1^{+} congenic recipients were irradiated with 2×550rad given 3h apart. Mice were analyzed 6 weeks following transfer.

STAT4 and STAT5 posphorylation—To assess STAT5 phosphorylation in splenic NK cells, splenocytes were counted and 2.5×10^{6} cells plated in 100μL culture medium in a round-bottom plate. The cells were rested for 1 hour at 37°C. Separately, serial 10-fold dilutions were made to prepare 2X IL-15/IL-15Rα stocks consisting of 200ng/mL to 0.02ng/mL and 60ng/mL to 0.006ng/mL in culture medium. At t=0, 100μL of the 2X

cytokine mix was added to the splenocytes and mixed, covering a final range of 100ng/mL to 0.003ng/mL IL-15/IL-15Rα, and incubated for 1 hour at 37°C. Cells were fixed by adding 50μL of 10% Paraformaldehyde (Electron Microscopy Sciences) and incubating 15 minutes at 37°C. The fixed cells were pelleted and washed 2x with FACS buffer. The fixed cells were placed on ice and permeabilized by adding 100μL of ice-cold methanol and incubated for 30 minutes at −20°C. The cells were thoroughly washed 2x with FACS buffer and subsequently stained for flow cytometry. For STAT4 phosphorylation, splenocytes were plated and rested as above for 1h at 37°C, then stimulated with 20ng/mL of IL-12 for the indicated times and processed as above.

***In vitro* stimulation and NK cell expansion—**Sorted splenic NK cells were expanded in NK cell culture medium (RPMI+ 10% FBS+ 1X Penicillin/Streptomycin+ 1X 2-Mercaptoethanol (Gibco)), and supplemented with 20ng/mL recombinant IL-15/IL-15Rα complexes for 7–8 days. For *Id2* and *Rroid* induction, expanded NK cells were washed 2x in PBS and 5×10^5 cells were plated 500μL of culture medium without cytokines and allowed to rest at 37°C for 4 or 5 hours. Following this period, 500uL of pre-warmed culture media containing IL-15/IL-15Rα complexes to a final concentration of either 0.5ng/mL or 5ng/mL IL-15/IL-15Rα complexes and cultured for an additional 3h.

For *in vitro* T cell stimulation, 2×10^5 sorted splenic $CD4^+$ or $CD8^+$ T cells were plated in T cell culture medium (RPMI+ 10% FBS+ 20mM HEPES+ 1X L-Glutamine (ThermoFisher Scientific)+ 1X Sodium Pyruvate (ThermoFisher Scientific)+ 1X 2-Mercaptoethanol+ 1X Nonessential amino acids (ThermoFisher Scientific)+ 1X Penicillin/Streptomycin) in 48 well plates pre-coated overnight with 5μg/mL anti-CD3 (145-2C11, ThermoFisher Scientific) and 1 μg/mL soluble anti-CD28 (37.51, ThermoFisher Scientific). For Th0 conditions, the media was supplemented with 100U/mL recombinant human IL-2; for Th1-skewing conditions, the media contained 100U/mL IL-2+ 20ng/mL IL-12, and 10ng/mL anti-IL-4. For $CD8^+$ T cells, the media contained 100U/mL IL-2.

***In vitro* locked nucleic acid treatment—**For *in vitro Rroid* knockdown by locked nucleic acids (LNAs), we first sorted and expanded splenic NK cells as described above. After collection, 4×10^6 NK cells were combined with 4μM control LNA or a mix of four LNAs specifically targeting *Rroid* and transfected via nucleofection in an Amaxa Nucleofector 2b device using the Mouse T cell Nucleofector kit (Lonza) according to the manufacturer's instructions and maintained in NK cell culture medium supplemented with IL-15/IL-15Rα complexes for the indicated times.

RNA isolation, cDNA synthesis, and qPCR—Total RNA was isolated from mouse tissues or sorted cells using TRIzol (ThermoFisher Scientific) according to the manufacturer's instructions. Glycogen (Roche) was used as a carrier. Isolated total RNA was quantified using a Nanodrop 1000. cDNA was synthesized using SuperScript II Reverse Transcriptase (ThermoFisher Scientific) according to the manufacturer's instructions using oligo-dT primers. qPCR was performed using SYBR Green (KAPA SYBR Fast; KAPA Biosystems) using the indicated primers. In some experiments, 2500 liver ILC1s or NK cells were sorted and used as input for the Cells-to-Ct 1-step Taqman qPCR kit (ThermoFisher Scientific). All qPCR reactions were performed in duplicate or triplicate on a CFX96 Touch

system (Bio-Rad) or ViiA7 Real-Time PCR instrument (ThermoFisher Scientific). The primers used for qPCR are listed in Table S2.

ChIP-qPCR—Splenic NK cells for ChIP-qPCR on histone marks were expanded *in vivo* using IL-2/αIL-2 complexes and sorted to high purity. To assess STAT5 recruitment to the *Id2* promoter, NK cells were expanded *in vitro* as described, rested, and stimulated for 1 hour with 20ng/mL IL-15/IL-15Rα complexes before fixation. NK cells were collected and fixed with 1% Paraformaldehyde for 5 minutes at room temperature, and the reaction was quenched by the addition of 0.125M glycine. The fixed cells were washed twice with ice cold PBS and nuclei were prepared by incubating with lysing buffer (50mM Tris, pH 8.0+140mM NaCl+1mM EDTA, pH 8.0+10% Glycerol+0.5% NP-40+0.25% Triton X-100) for 10 minutes on ice. The nuclei were then washed twice with 10mM Tris, pH 8.1+200mM NaCl+1mM EDTA, pH8.0. Nuclei were resuspended in shearing buffer (10mM Tris, pH 8.1+1mM EDTA, pH8.0+ 0.1% SDS) and sonicated 90 seconds using a Covaris S220 (140W, 10% duty factor, 200 cycles per burst) to obtain ~400–500bp fragments. Sheared chromatin aliquots containing an equivalent 1×10^6 nuclei were flash frozen and stored at −80°C.

For ChIP-qPCR on histone marks, an equivalent of 1×10^6 nuclei of sheared chromatin was used as input and diluted to 1mL using IP dilution buffer (20mM Tris, pH8.1+ 2mM EDTA, pH8.0+ 150mM NaCl+ 1% Triton X-100+ 0.01%SDS). For STAT5 pulldown, 3×10^6 nuclei were used. Protein G magnetic beads (ThermoFisher Scientific) were pre-loaded with 1.5μg of anti-H3K27ac (ab4729; Abcam), anti-H3K36me3 (ab9050; Abcam), or 5μg of anti-STAT5A/B (AF2168; R&D Systems) and incubated with the chromatin overnight at 4°C. Beads were washed once in low salt buffer (20mM Tris, pH8.1+ 2mM EDTA+ 50mM NaCl + 1% Triton X-100+ 0.1% SDS), once in high salt buffer (20mM Tris, pH8.1+ 2mM EDTA + 500mM NaCl+ 1% Triton X-100+ 0.1% SDS), once in LiCl buffer (10mM Tris, pH 8.1+ 1mM EDTA+ 0.25mM LiCl+ 1% NP-40+ 1% deoxycholic acid) and twice in TE buffer (10mM Tris-HCl, pH8.0+ 1mM EDTA). Washed beads were eluted twice with 100 μL of elution buffer (1% SDS+ 0.1M $NaHCO_3$) and de-crosslinked (0.1 mg/ml RNase, 0.3 M NaCl and 0.3 mg/ml Proteinase K) overnight at 65°C. The samples were purified with Qiaquick PCR columns (Qiagen). qPCR was performed in triplicate using KAPA SYBR Fast on a ViiA7 Real-Time PCR instrument (ThermoFisher Scientific) using the primers listed in Table S2.

Chromatin Conformation Capture (3C)—To prepare nuclei for 3C assays, splenic NK cells were sorted and expanded for 7 days. Cells were fixed at room temperature for 10min at a concentration of 10×10^6 cells/mL in 2% Paraformaldehyde in PBS, then the reaction was quenched with the addition of 0.125M glycine and placed on ice for 10 minutes. The cells were pelleted and nuclei collected by incubating in lysing buffer (50mM Tris, pH 8.0+140mM NaCl+1mM EDTA, pH 8.0+10% Glycerol+0.5% NP-40+0.25% Triton X-100) for 20 minutes on ice. Lysis was monitored by methyl-green pyronin staining (Bio-rad). The nuclei were pelleted, snap frozen, and stored at −80°C.

For 3C assays, nuclei were thawed and resuspended in 500μL 1X NEBuffer 2.1. To lyse the nuclei and strip chromatin-bound proteins, 2.5μL of 20% SDS was added and nuclei were

incubated for 10min at 65°C; the reaction was quenched with the addition of 26.5μL of 20% Triton X-100 and incubated for 1h at 37°C with shaking at 120rpm. 500U of HindIII-HF was then added and the nuclei were digested overnight at 37°C with shaking at 120rpm. This reaction was stopped by the addition of 40μL of 20% SDS and incubating 25min at 65°C. The nuclei were transferred to a 50mL conical tube and diluted with 6.125mL ligation buffer. 375μL of 20% Triton X-100 was added and the nuclei were incubated for 1h at 37°C. The nuclei were then ligated for five hours with 6667 Cohesive End Units of T4 DNA Ligase (NEB) at 16°C with shaking at 120rpm. Crosslinks were reversed by addition of 100uL of 10mg/mL Proteinase K (Roche) overnight at 65°C. The template was then treated with RNase A for 30min at 37°C with shaking at 120rpm. The 3C template was then purified with saturated phenol-chloroform (Sigma) extraction. Digestion efficiency was confirmed by qPCR after sampling the template before and after digestion, reversing crosslinks, and extracting the DNA.

To control for PCR efficiency, two BACs containing the loci of interest (RP23-300A18 and RP23-342B; Bacpac) were mixed at equimolar concentrations and digested overnight with 500U of HindIII-HF. The digested BAC template was then extracted via saturated phenol-chloroform, brought up in 200uL of ligase buffer, and ligated overnight in 6667 Cohesive End Units of T4 DNA ligase overnight at 16°C. The BAC template was then isolated by saturated phenol-chloroform extraction. Both BAC and 3C ligation products were amplified by qPCR using SYBR Fast Master Mix on a CFX96 Touch System. The products were visualized on a 2% agarose gel, imaged using a ChemiDoc MP system, and band intensity was quantified using Fiji (Schindelin et al., 2012). The band intensity of 3C products was normalized to that of the respective BAC control product.

RNA-seq—The RNA-seq tracks in Figure 1A were from GSE77695 (Shih et al., 2016). For RNA-seq from *Rroid*$^{-/-}$ NK cells, total RNA was isolated from sorted CD27^{+} CD11b^{+} NK cells using a combination of TRIzol and RNeasy Micro columns (Qiagen). The aqueous phase from the TRIzol-chloroform extraction was precipitated with ethanol, applied to RNeasy Micro columns and processed according to the manufacturer's instructions. The RNA libraries were generated using the Ovation RNA-Seq System V2 (Nugen) and the KAPA Hyper Prep Kit (KAPA Biosystems). Sequencing was performed on the HiSeq2500. The resulting reads were trimmed and aligned to the NCBIM37/mm9 genome using Tophat2. Transcript counts were generated using HTSeq and differential gene analysis was performed using DESeq2.

To identify Id2-dependent genes for GSEA, RNA-seq reads from GSE76466 (Delconte et al., 2016) were analyzed using Tophat2, HTSeq, and DESeq2 as described previously. Up- and downregulated differentially expressed genes (FDR<0.05) were used as input gene sets. GSEA was performed using gseapy.

ATAC-seq and peak calling—The ATAC-seq tracks in Figures 1A, 6C, S1A, and S5 were from GSE77695 (Shih et al., 2016). ATAC-seq for *Rroid*$^{-/-}$ NK cells was done on Illumina NextSeq at a sequencing depth of ~60–70 million reads per sample. Libraries were prepared in triplicate. 2×75 bp paired end reads were mapped to the mouse mm9 reference genome using 'bwa' algorithm with 'mem' option with default parameters (Li and Durbin,

2009). Only reads that uniquely mapped to the genome were used in subsequent analysis. Duplicate reads were eliminated to avoid potential PCR amplification artifacts and to eliminate high number of mtDNA duplicates observed in ATAC-seq libraries. Post-alignment filtering resulted in ~30–40 million uniquely aligned singleton reads. ATAC-seq enriched regions (peaks) in each sample was identified using MACS2 (Zhang et al., 2008). Only peaks called with a peak score (q-value) of 1% or better were used in downstream analysis. Peak annotation was performed via HOMER v4.6 annotatePeaks.pl (Heinz et al., 2010) for the mm9 assembly. Differentially open chromatin loci were identified using R Bioconductor DiffBind package.

Transcription factor footprinting—For transcription factor (TF) footprinting, we used the Protein Interaction Quantification (PIQ) algorithm (Sherwood et al., 2014) to quantify TF binding events based on ATAC-seq chromatin accessibility profiles. We merged JASPAR motifs (Mathelier *et al.*, 2013) with SELEX-based motifs (Ogawa and Biggin, 2012) and generated a set of 480 TFs as input to PIQ footprint calls. For each putative TF binding event, PIQ outputs a purity score reflecting the probability of TF binding to that locus. We have included only footprint calls with >0.9 purity score in the subsequent analyses.

QUANTIFICATION AND STATISTICAL ANALYSIS

Statistical analyses were performed in Prism 7 using unpaired, two-tailed Student's *t*-test or one way ANOVA with Tukey's post hoc, as indicated. In all cases $p \leq 0.05$ was considered statistically significant. All error bars represent S.E.M.

DATA AND SOFTWARE AVAILABILITY

The raw data for the RNA-seq and ATAC-seq reported in this manuscript have been deposited in GEO under the accession number GSE101459

Supplementary Material

Refer to Web version on PubMed Central for supplementary material.

Acknowledgments

We thank C. Hunter for providing *Tbx21*$^{-/-}$ mice, and J. Kurachi for technical support. The work in this manuscript was supported by funds from CHOP, UPenn IFI and IDOM pilot projects, and NIH R21AI128060, R21DK111755, and R01HL136572 (J.H.M.); A.W. and R.A.F. were supported by NIH R21AI110776; R.A.F. by the Howard Hughes Medical Institute; I.E.B. by NIH R01AI103062 and R01AI128530; W.K.M. by NIH T32AI055428 and F31AI124538; J.J.K. by NIH T32DK007780; S.P.S. by NIH F30DK094708; and A.R. and M.C.D. by New Innovator NIH DP2OD008514, NIH R33EB019767, and NSF CAREER 1350601. E.J.W. is a member of the Parker Institute for Cancer Immunotherapy, which supports the Penn Cancer Immunotherapy Program. H.V.-F. is funded by ERC (647274), EU; Kenneth Rainin Foundation, US; Crohn's and Colitis Foundation of America, US; and FCT, Portugal.

References

Anderson KM, Anderson DM, McAnally JR, Shelton JM, Bassel-Duby R, Olson EN. Transcription of the non-coding RNA upperhand controls Hand2 expression and heart development. Nature. 2016; 539:433–436. [PubMed: 27783597]

Artis D, Spits H. The biology of innate lymphoid cells. Nature. 2015; 517:293–301. [PubMed: 25592534]

Bulger M, Groudine M. Functional and mechanistic diversity of distal transcription enhancers. Cell. 2011; 144:327–339. [PubMed: 21295696]

Busslinger GA, Stocsits RR, van der Lelij P, Axelsson E, Tedeschi A, Galjart N, Peters JM. Cohesin is positioned in mammalian genomes by transcription, CTCF and Wapl. Nature. 2017; 544:503–507. [PubMed: 28424523]

Carpenter S, Aiello D, Atianand MK, Ricci EP, Gandhi P, Hall LL, Byron M, Monks B, Henry-Bezy M, Lawrence JB, et al. A long noncoding RNA mediates both activation and repression of immune response genes. Science. 2013; 341:789–792. [PubMed: 23907535]

Chiossone L, Chaix J, Fuseri N, Roth C, Vivier E, Walzer T. Maturation of mouse NK cells is a 4-stage developmental program. Blood. 2009; 113:5488–5496. [PubMed: 19234143]

Constantinides MG, Gudjonson H, McDonald BD, Ishizuka IE, Verhoef PA, Dinner AR, Bendelac A. PLZF expression maps the early stages of ILC1 lineage development. Proc Natl Acad Sci U S A. 2015; 112:5123–5128. [PubMed: 25838284]

Constantinides MG, McDonald BD, Verhoef PA, Bendelac A. A committed precursor to innate lymphoid cells. Nature. 2014; 508:397–401. [PubMed: 24509713]

Cortez, Victor S., Cervantes-Barragan, L., Robinette, Michelle L., Bando, Jennifer K., Wang, Y., Geiger, Theresa L., Gilfillan, S., Fuchs, A., Vivier, E., Sun, Joe C., et al. Transforming Growth Factor-β Signaling Guides the Differentiation of Innate Lymphoid Cells in Salivary Glands. Immunity. 2016

Delconte, Rebecca B., Shi, W., Sathe, P., Ushiki, T., Seillet, C., Minnich, M., Kolesnik, Tatiana B., Rankin, Lucille C., Mielke, Lisa A., Zhang, J-G., et al. The Helix-Loop-Helix Protein ID2 Governs NK Cell Fate by Tuning Their Sensitivity to Interleukin-15. Immunity. 2016

Derrien T, Johnson R, Bussotti G, Tanzer A, Djebali S, Tilgner H, Guernec G, Martin D, Merkel A, Knowles DG, et al. The GENCODE v7 catalog of human long noncoding RNAs: analysis of their gene structure, evolution, and expression. Genome Res. 2012; 22:1775–1789. [PubMed: 22955988]

Eberl G, Marmon S, Sunshine MJ, Rennert PD, Choi Y, Littman DR. An essential function for the nuclear receptor RORgamma(t) in the generation of fetal lymphoid tissue inducer cells. Nat Immunol. 2004; 5:64–73. [PubMed: 14691482]

Engreitz JM, Haines JE, Perez EM, Munson G, Chen J, Kane M, McDonel PE, Guttman M, Lander ES. Local regulation of gene expression by lncRNA promoters, transcription and splicing. Nature. 2016; 539:452–455. [PubMed: 27783602]

Fathman JW, Bhattacharya D, Inlay MA, Seita J, Karsunky H, Weissman IL. Identification of the earliest natural killer cell-committed progenitor in murine bone marrow. Blood. 2011; 118:5439–5447. [PubMed: 21931117]

Fatica A, Bozzoni I. Long non-coding RNAs: new players in cell differentiation and development. Nat Rev Genet. 2014; 15:7–21. [PubMed: 24296535]

Gury-BenAri M, Thaiss CA, Serafini N, Winter DR, Giladi A, Lara-Astiaso D, Levy M, Salame TM, Weiner A, David E, et al. The Spectrum and Regulatory Landscape of Intestinal Innate Lymphoid Cells Are Shaped by the Microbiome. Cell. 2016

Heinz S, Benner C, Spann N, Bertolino E, Lin YC, Laslo P, Cheng JX, Murre C, Singh H, Glass CK. Simple combinations of lineage-determining transcription factors prime cis-regulatory elements required for macrophage and B cell identities. Mol Cell. 2010; 38:576–589. [PubMed: 20513432]

Henao-Mejia J, Williams A, Rongvaux A, Stein J, Hughes C, Flavell RA. Generation of Genetically Modified Mice Using the CRISPR-Cas9 Genome-Editing System. Cold Spring Harb Protoc. 2016; 2016 pdb prot090704.

Kee BL. E and ID proteins branch out. Nat Rev Immunol. 2009; 9:175–184. [PubMed: 19240756]

Klose CS, Flach M, Mohle L, Rogell L, Hoyler T, Ebert K, Fabiunke C, Pfeifer D, Sexl V, Fonseca-Pereira D, et al. Differentiation of type 1 ILCs from a common progenitor to all helper-like innate lymphoid cell lineages. Cell. 2014; 157:340–356. [PubMed: 24725403]

Klose CS, Kiss EA, Schwierzeck V, Ebert K, Hoyler T, d'Hargues Y, Goppert N, Croxford AL, Waisman A, Tanriver Y, Diefenbach A. A T-bet gradient controls the fate and function of CCR6-RORgammat+ innate lymphoid cells. Nature. 2013; 494:261–265. [PubMed: 23334414]

Kotzin JJ, Spencer SP, McCright SJ, Kumar DB, Collet MA, Mowel WK, Elliott EN, Uyar A, Makiya MA, Dunagin MC, et al. The long non-coding RNA Morrbid regulates Bim and short-lived myeloid cell lifespan. Nature. 2016; 537:239–243. [PubMed: 27525555]

Kurachi M, Barnitz RA, Yosef N, Odorizzi PM, DiIorio MA, Lemieux ME, Yates K, Godec J, Klatt MG, Regev A, et al. The transcription factor BATF operates as an essential differentiation checkpoint in early effector CD8+ T cells. Nat Immunol. 2014; 15:373–383. [PubMed: 24584090]

Lam MT, Li W, Rosenfeld MG, Glass CK. Enhancer RNAs and regulated transcriptional programs. Trends Biochem Sci. 2014; 39:170–182. [PubMed: 24674738]

Lara-Astiaso D, Weiner A, Lorenzo-Vivas E, Zaretsky I, Jaitin DA, David E, Keren-Shaul H, Mildner A, Winter D, Jung S, et al. Immunogenetics. Chromatin state dynamics during blood formation. Science. 2014; 345:943–949. [PubMed: 25103404]

Li H, Durbin R. Fast and accurate short read alignment with Burrows-Wheeler transform. Bioinformatics. 2009; 25:1754–1760. [PubMed: 19451168]

Masson F, Minnich M, Olshansky M, Bilic I, Mount AM, Kallies A, Speed TP, Busslinger M, Nutt SL, Belz GT. Id2-mediated inhibition of E2A represses memory CD8+ T cell differentiation. J Immunol. 2013; 190:4585–4594. [PubMed: 23536629]

Merkenschlager M, Nora EP. CTCF and Cohesin in Genome Folding and Transcriptional Gene Regulation. Annu Rev Genomics Hum Genet. 2016; 17:17–43. [PubMed: 27089971]

Moro K, Yamada T, Tanabe M, Takeuchi T, Ikawa T, Kawamoto H, Furusawa J, Ohtani M, Fujii H, Koyasu S. Innate production of T(H)2 cytokines by adipose tissue-associated c-Kit(+)Sca-1(+) lymphoid cells. Nature. 2010; 463:540–544. [PubMed: 20023630]

Ogawa N, Biggin MD. High-throughput SELEX determination of DNA sequences bound by transcription factors in vitro. Methods Mol Biol. 2012; 786:51–63. [PubMed: 21938619]

Polansky JK, Bahri R, Divivier M, Duitman EH, Vock C, Goyeneche-Patino DA, Orinska Z, Bulfone-Paus S. High dose CD11c-driven IL15 is sufficient to drive NK cell maturation and anti-tumor activity in a trans-presentation independent manner. Sci Rep. 2016; 6:19699. [PubMed: 26822794]

Rinn JL, Chang HY. Genome regulation by long noncoding RNAs. Annu Rev Biochem. 2012; 81:145–166. [PubMed: 22663078]

Schindelin J, Arganda-Carreras I, Frise E, Kaynig V, Longair M, Pietzsch T, Preibisch S, Rueden C, Saalfeld S, Schmid B, et al. Fiji: an open-source platform for biological-image analysis. Nat Methods. 2012; 9:676–682. [PubMed: 22743772]

Sherwood RI, Hashimoto T, O'Donnell CW, Lewis S, Barkal AA, van Hoff JP, Karun V, Jaakkola T, Gifford DK. Discovery of directional and nondirectional pioneer transcription factors by modeling DNase profile magnitude and shape. Nat Biotechnol. 2014; 32:171–178. [PubMed: 24441470]

Shih HY, Sciume G, Mikami Y, Guo L, Sun HW, Brooks SR, Urban JF Jr, Davis FP, Kanno Y, O'Shea JJ. Developmental Acquisition of Regulomes Underlies Innate Lymphoid Cell Functionality. Cell. 2016; 165:1120–1133. [PubMed: 27156451]

Shlyueva D, Stampfel G, Stark A. Transcriptional enhancers: from properties to genome-wide predictions. Nat Rev Genet. 2014; 15:272–286. [PubMed: 24614317]

Spits H, Bernink JH, Lanier L. NK cells and type 1 innate lymphoid cells: partners in host defense. Nat Immunol. 2016; 17:758–764. [PubMed: 27328005]

Takada H, Matsuzaki G, Hiromatsu K, Nomoto K. Analysis of the Role of Natural-Killer-Cells in Listeria-Monocytogenes Infection - Relation between Natural-Killer-Cells and T-Cell Receptor-Gamma-Delta T-Cells in the Host-Defense Mechanism at the Early-Stage of Infection. Immunology. 1994; 82:106–112. [PubMed: 8045587]

Viegas N, Andzinski L, Wu CF, Komoll RM, Gekara N, Dittmar KE, Weiss S, Jablonska J. IFN-gamma production by CD27(+) NK cells exacerbates Listeria monocytogenes infection in mice by inhibiting granulocyte mobilization. Eur J Immunol. 2013; 43:2626–2637. [PubMed: 23818011]

Villarino A, Laurence A, Robinson GW, Bonelli M, Dema B, Afzali B, Shih HY, Sun HW, Brooks SR, Hennighausen L, et al. Signal transducer and activator of transcription 5 (STAT5) paralog dose governs T cell effector and regulatory functions. Elife. 2016:5.

Vivier E, van de Pavert SA, Cooper MD, Belz GT. The evolution of innate lymphoid cells. Nat Immunol. 2016; 17:790–794. [PubMed: 27328009]

Yang Q, Monticelli LA, Saenz SA, Chi AW, Sonnenberg GF, Tang J, De Obaldia ME, Bailis W, Bryson JL, Toscano K, et al. T cell factor 1 is required for group 2 innate lymphoid cell generation. Immunity. 2013; 38:694–704. [PubMed: 23601684]

Zhang Y, Liu T, Meyer CA, Eeckhoute J, Johnson DS, Bernstein BE, Nussbaum C, Myers RM, Brown M, Li W, Liu XS. Model-based Analysis of ChIP-Seq (MACS). Genome Biology. 2008:9.

Zook EC, Kee BL. Development of innate lymphoid cells. Nature Immunology. 2016; 17:775–782. [PubMed: 27328007]

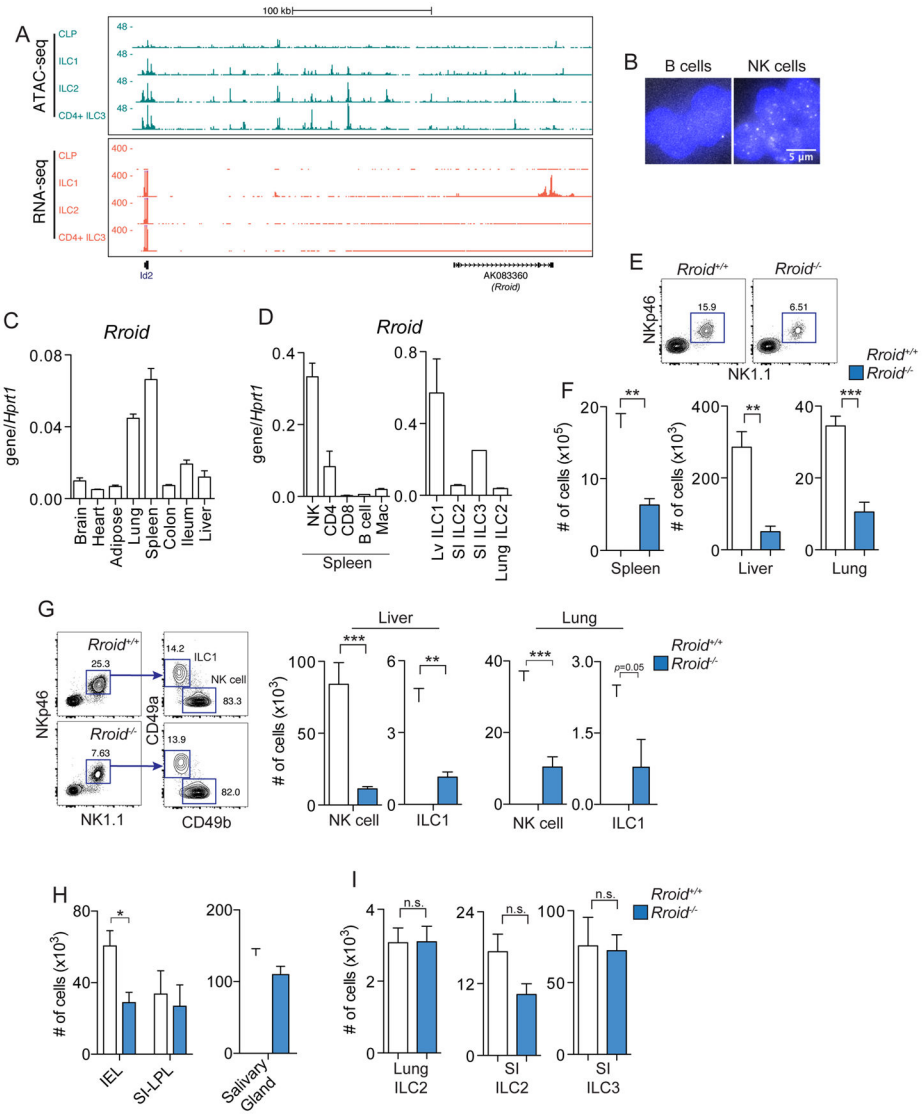

Figure 1. The *Rroid* locus controls peripheral group 1 ILC homeostasis

A. Gene browser tracks of ATAC-seq (top) and RNA-seq (bottom) from indicated cell populations.

B. RNA fluorescence *in-situ* hybridization (FISH) of *Rroid* RNA in sort-purified CD19$^+$ B cells and CD3, CD5$^-$ NK1.1$^+$ NKp46$^+$ NK cells. Cells were probed for *Rroid* using Cy3-labeled probes (white). Nuclei were visualized with DAPI (blue).

C. *Rroid* expression in indicated mouse tissues was determined by quantitative PCR (qPCR). Normalized to *Hprt* expression. (n=3 mice per group). Data are representative of two independent experiments.

D. *Rroid* expression by qPCR in sorted cell populations from spleen, liver (Lv), small intestine lamina propria (SI), and lung parenchyma (n=3 mice per group; liver populations represent n=2 of 5 pooled mice each). Normalized to *Hprt* expression. Data are pooled from multiple independent experiments.

E. Representative flow cytometry plots of NK1.1$^+$ NKp46$^+$ cells in *Rroid*$^{+/+}$ and *Rroid*$^{-/-}$ mice isolated from lung tissue. (Gated on live, CD45.2$^+$ CD3, CD5$^-$ cells).

F. Absolute numbers of CD3, CD5$^-$ NK1.1$^+$ NKp46$^+$ cells in indicated mouse tissues (n=4 mice per group). Data are representative of three independent experiments.

G. Gating strategy (left) to identify CD49a$^+$ ILC1s and CD49b$^+$ NK cells in mouse liver. Cells were pre-gated on CD45.2$^+$ CD3, CD5$^-$ cells. Absolute numbers of liver and lung NK cells and ILC1s (right; n=4 mice per group). Data are representative of three independent experiments.

H. Absolute numbers of Lin$^-$ CD45.2$^+$ CD90.2$^+$ Rorγt$^-$ Eomes$^-$ T-bet$^+$ ILC1s in the small intestine intraepithelial lymphocyte (IEL) and lamina propria (SI-LPL) compartments (left) and salivary gland CD3, CD5$^-$ CD45.2$^+$ CD49b$^+$ CD49a$^+$ ILC1s (right). (n=3–4 mice per group). Data are representative of two to three independent experiments.

I. Absolute numbers of ILC2 and ILC3 populations from indicated tissues (n=3–5 mice per group). Intestinal ILC2s were Lin$^-$ CD45.2$^+$ CD90.2$^+$ GATA3$^+$ Rorγt$^-$; ILC3s were Lin$^-$ CD45.2$^+$ CD90.2$^+$ GATA3$^-$ Rorγt$^+$. Lung ILC2 were Lin$^-$ CD45.2$^+$ CD90.2$^+$ T1/ST2$^+$. Data are representative of three independent experiments.

$*p \leq 0.05$, $**p \leq 0.01$, $***p \leq 0.001$. Two-tailed t-test. All error bars represent SEM. See also Figure S1.

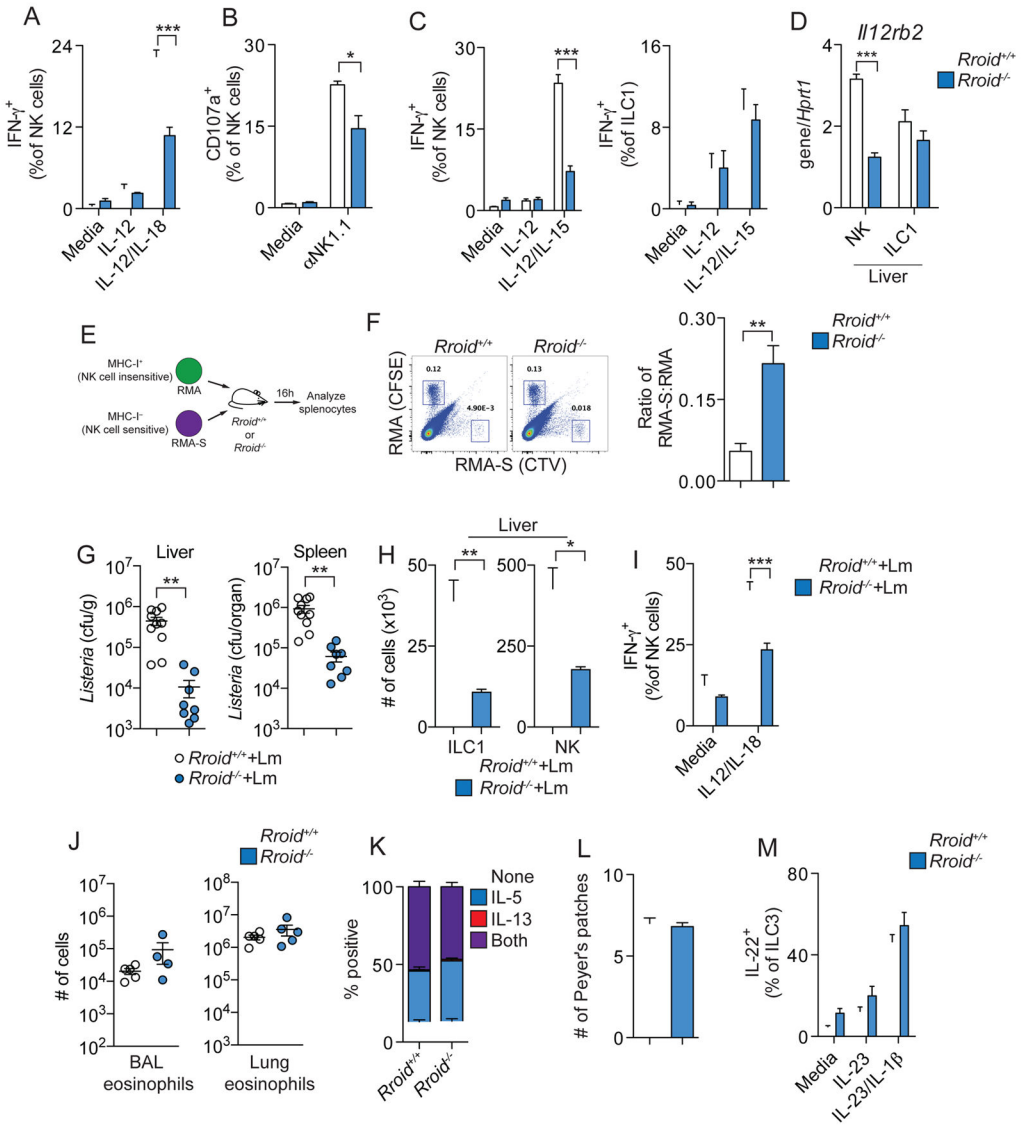

Figure 2. The *Rroid* locus is necessary for NK cell function

A. IFN-γ production in splenic NK cells. Splenocytes were stimulated for 4h *ex vivo* with 20ng/mL IL-12, a combination of IL-12 and 20ng/mL IL-18, or with media alone (U/S). Data are representative of three independent experiments.

B. NK cell degranulation as measured by CD107a staining in splenocytes activated by anti-NK1.1 for 4h *ex vivo*. Data are representative of two independent experiments.

C. IFN-γ production in liver NK cells (left) or ILC1s (right). Liver lymphocytes were stimulated for 4h *ex vivo* with 20ng/mL IL-12, a combination of IL-12 and 20ng/mL IL-15/IL-15Rα complex, or media alone (U/S, n=3–4 mice per group). Data are representative of two independent experiments.

D. Expression of *Il12rb2* by qPCR in liver NK cells and ILC1s. 2500 NK cells and ILC1s were sorted from the liver and subjected to 1-step qRT-PCR. Data are normalized to *Hprt1* expression. (n=3 mice per group).

E. Experimental outline of the RMA-S transfer system to probe NK cell function *in vivo*. 5×10^6 CFSE-labeled RMA cells (MHC-I^+) and 15×10^6 CTV-labeled RMA-S (MHC-I^-) cells were combined were injected intravenously into recipients, and splenocytes were analyzed 16h after injection.

F. Gating strategy for identifying fluorescently-labeled RMA and RMA-S cells in the spleen (left). Ratio of RMA-S:RMA cell numbers (right, n=6 mice from two pooled independent experiments).

G. *Listeria monocytogenes* (Lm) burden in the liver (left) and spleen (right). Mice were infected intravenously with 3×10^4 CFU of *Listeria* and analyzed 3d post infection (n=8–9 mice per group). Data are representative of two independent experiments.

H. Absolute numbers of ILC1 (left) and NK cells (right) in the livers of *Rroid*$^{-/-}$ mice and controls 3d post infection with *Listeria* (n=4–5 mice per group).

I. Production of IFN-γ from splenic NK cells in mice 3d post infection with *Listeria*. Cells were stimulated 4h with 20ng/mL IL-12, a combination of IL-12 and 20ng/mL IL-18, or with media alone. (n=4–5 mice per group).

J. Absolute numbers of eosinophils (CD45$^+$ CD11c$^-$ Siglec-F$^+$) in the bronchoalveolar lavage (BAL) and lung parenchyma of mice challenged intranasally with 30μg papain every 24h for 5 days (n=4–5 mice per group).

K. ILC2 cytokine production from mice challenged with papain. Lung lymphocytes were stimulated 4h with PMA/Ionomycin and gated on CD45$^+$ CD3, CD5, CD19$^-$ CD90.2$^+$ T1/ST2$^+$ cells (n=5 mice per group).

L. Enumeration of Peyer's patches in the small intestine of *Rroid*$^{+/+}$ and *Rroid*$^{-/-}$ mice (n=10 mice per group pooled from three independent experiments).

M. IL-22 production in small intestine ILC3s. Lymphocytes from small intestine were stimulated 4h with media alone (U/S), IL-23 (20ng/mL), or IL-23 and IL-1β (10ng/mL) (n=4 mice per group). Representative of two independent experiments.

$*p\leq0.05$, $**p\leq0.01$, $***p\leq0.001$. Two-tailed t-test. All error bars represent SEM. See also Figure S2.

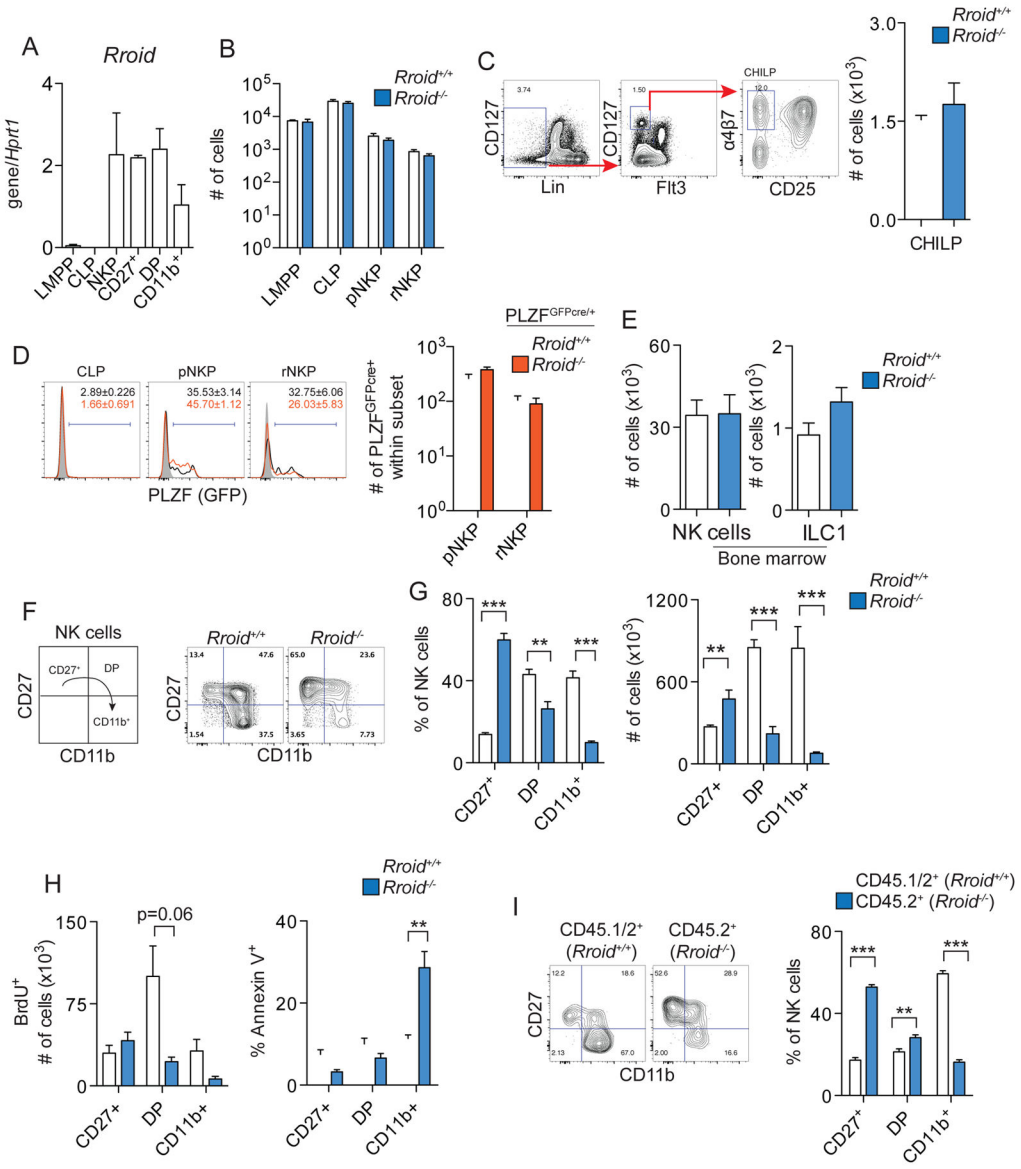

Figure 3. *Rroid* promotes the maturation of group 1 ILCs

A. *Rroid* expression in NK cells and progenitors. Lymphoid-primed multipotent progenitors (LMPP), common lymphoid progenitors (CLP), and NK cell progenitors (NKP) sorted from bone marrow; $CD27^+$, double positive (DP, $CD27^+$, $CD11b^+$), and $CD11b^+$ NK cells sorted from spleen and *Rroid* expression was quantified by qPCR (LMPP, CLP, and NKP populations are n=2 of 5 pooled mice each, and splenic NK cells are n=3). Normalized to *Hprt* expression.

B. Absolute numbers of LMPP, CLP, pre-NK progenitor (pNKP), and refined NK progenitor (rNKP) populations in bone marrow (n=3 mice per group). Data are representative of two independent experiments.

C. Gating strategy for identifying common helper ILC progenitors (CHILP) in the bone marrow (left). Absolute numbers of CHILP in $Rroid^{+/+}$ and $Rroid^{-/-}$ mice (right; n=4 mice per group). Representative of two independent experiments.

D. Histogram depicting the frequency±SEM of ILC progenitors marked by PLZF expression in CLP, pNKP, and rNKP populations (left), and absolute numbers of $PLZF^+$ cells within pNKP and rNKP subsets (right). Shaded histograms are GFP-negative controls (n=3–4 mice per group from two pooled experiments).

E. Absolute numbers of bone marrow NK cells and ILC1s (n=3 mice per group). Data are representative of three independent experiments.

F. Schematic (left) and flow plots (right) depicting maturation pathway in splenic NK cells in *Rroid*$^{+/+}$ and *Rroid*$^{-/-}$ mice. Gated on $CD45.2^+$ CD3, $CD5^-$ $NK1.1^+$ $NKp46^+$ cells.

G. Frequency (left) and absolute numbers (right) of NK cell maturation in the spleen of *Rroid*$^{+/+}$ and *Rroid*$^{-/-}$ mice (n=4 mice per group). Data are representative of four independent experiments.

H. BrdU incorporation (left) and Annexin V staining (right) of maturing splenic NK cells. Mice were injected i.p. every 12h with 1mg BrdU for 3d. Splenocytes were either fixed and probed for BrdU incorporation or stained with Annexin V to determine cell viability (n=3–4 mice per group). Data are representative of two independent experiments.

I. Flow cytometry plot (left) and frequency (right) of maturing splenic NK cells in competitive bone marrow chimeras analyzed 8 weeks post-transfer (n=8 mice per group). Data are pooled from two independent experiments.

$*p \leq 0.05$, $**p \leq 0.01$, $***p \leq 0.001$. Two-tailed t-test. All error bars represent SEM. See also Figure S3.

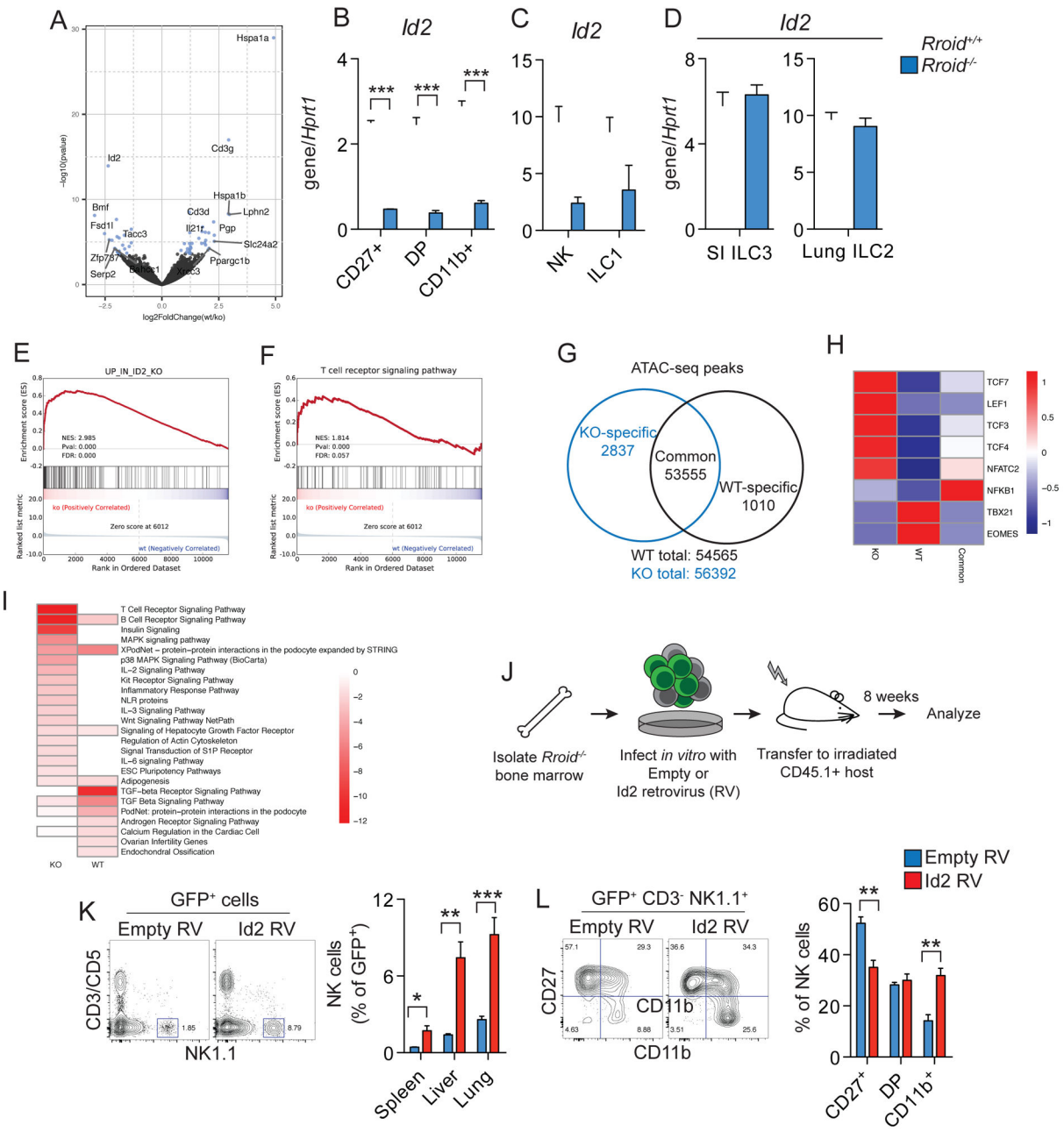

Figure 4. *Rroid* promotes group 1 ILC maturation and lineage identity through *Id2*

A. Volcano plot of RNA-seq results in sorted splenic DP (CD27$^+$, CD11b$^+$) *Rroid*$^{+/+}$ and *Rroid*$^{-/-}$ NK cells. Genes with FDR<0.05 are depicted in blue (n=3 mice per group).

B. *Id2* expression in maturing NK cell populations sorted from spleen and analyzed by qPCR (n=3 mice per group). Normalized to *Hprt* expression. Data are representative of two independent experiments.

C. qPCR of *Id2* expression in sorted liver NK cells and ILC1s (n=2 of 5 pooled mice per group). Normalized to *Hprt* expression.

D. *Id2* expression in sorted ILC3s from small intestine (left) or IL-33 expanded ILC2s from lung (right) analyzed by qPCR (For ILC3s, n=4 mice per group pooled from two experiments; for ILC2s, n=5 mice per group from one experiment). ILC2s were expanded by intranasal administration of 250ng IL-33 daily for 4 days and sorted 24 hours following the last injection. Normalized to *Hprt* expression.

E. Gene Set Enrichment Analysis (GSEA) depicting enrichment of known *Id2*-regulated genes in *Rroid*$^{-/-}$ NK cells.

F. GSEA depicting enrichment of KEGG T cell receptor signaling pathway genes in *Rroid*$^{-/-}$ NK cells.

G. Venn diagram depicting unique ATAC-seq peaks called in sorted splenic *Rroid*$^{+/+}$ and *Rroid*$^{-/-}$ NK cells (n=3 mice per group).

H. Heatmap of transcription factor footprinting analysis. *Rroid*$^{+/+}$ and *Rroid*$^{-/-}$-specific ATAC-seq peaks were subjected to transcription factor footprinting analysis by the Protein Interaction Quantitation (PIQ) algorithm.

I. Enrichment of cellular pathways associated with open chromatin elements in *Rroid*$^{+/+}$ and *Rroid*$^{-/-}$ NK cells.

J. Schematic of *Id2* transduction experiment. *Rroid*$^{-/-}$ bone marrow was transduced *in vitro* with retrovirus bearing *Id2* or empty vector control and used to reconstitute lethally irradiated CD45.1^{+} hosts. Transduced cells were identified by expression of GFP.

K. NK cells as a proportion of GFP^{+} cells in bone marrow chimeras reconstituted with either empty retrovirus or Id2 retrovirus (n=4 mice per group).

L. Frequency of maturing splenic NK cells in bone marrow chimeras reconstituted with either empty retrovirus or Id2 retrovirus (n=4 mice per group).

$*p \leq 0.05$, $**p \leq 0.01$, $***p \leq 0.001$. Two-tailed t-test. All error bars represent SEM. See also Figure S4 and Table S1.

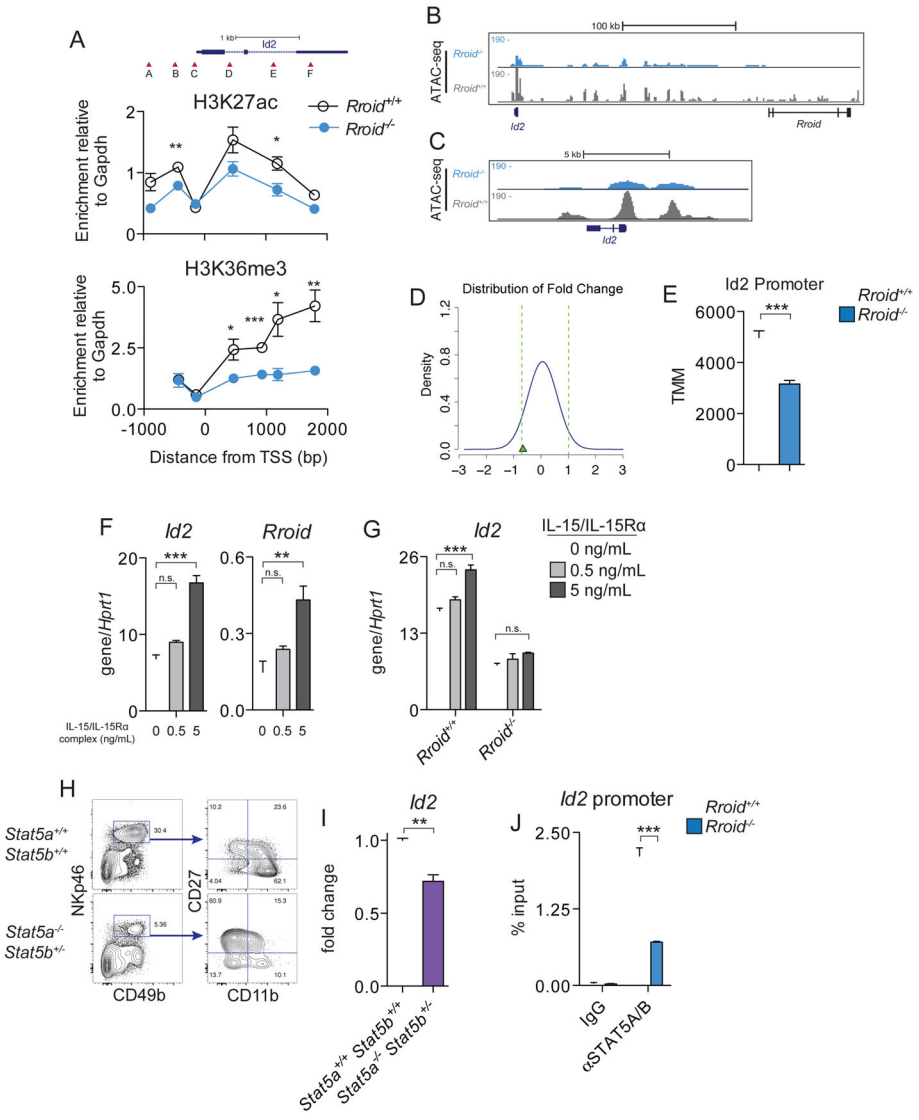

Figure 5. The *Rroid* locus promotes open chromatin and STAT5 deposition at the *Id2* promoter

A. Histone modifications at the *Id2* locus. Gene browser depiction of *Id2* locus and ChIP-qPCR primer locations (above). ChIP-qPCR showing H3K27ac and H3K36me3 enrichment within the *Id2* promoter and gene body (below). NK cells were expanded *in vivo* with IL-2/αIL-2 complexes and sorted from spleen (n=3 groups of 2 pooled mice per group). Results were normalized to enrichment at the *Gapdh* locus. Data are representative of two independent experiments.

B. Representative gene browser tracks of ATAC-seq reads at the *Id2* and *Rroid* loci in *Rroid*$^{+/+}$ and *Rroid*$^{-/-}$ NK cells.

C. Representative gene browser tracks of ATAC-seq reads at the *Id2* locus in *Rroid*$^{+/+}$ and *Rroid*$^{-/-}$ NK cells.

D. Density plot of $\log_2$ fold change distribution for ATAC-seq peaks in *Rroid*$^{+/+}$ and *Rroid*$^{-/-}$ NK cells. Fold changes were estimated as the ratio of the trimmed mean of M-values (TMM)-normalized read counts in consensus peak regions via the DiffBind R

package. Vertical dashed lines show the 5th and 95th percentiles. The green arrowhead shows the *Id2* promoter.

E. Relative chromatin accessibility at the *Id2* locus in *Rroid*$^{+/+}$ and *Rroid*$^{-/-}$ NK cells. Chromatin accessibility is depicted as an average of TMM-normalized read counts across replicates. Statistics were obtained using the DiffBind R package (n=3 mice per group).

F. *Id2* (left) and *Rroid* (right) expression in *in vitro* expanded NK cells stimulated with IL-15. Splenic NK cells were sorted and expanded 7d *ex vivo*. Prior to the experiment, cells were rested in culture media without cytokines media for 5h. Either media alone (0ng/mL), 0.5ng/mL, or 5ng/mL IL-15/IL-15Rα complex was added and cultured for an additional 3h. Gene expression was analyzed by qPCR. Results are normalized to *Hprt* (n=3 biological replicates per group).

G. qPCR analysis of *Id2* expression in *Rroid*$^{+/+}$and *Rroid*$^{-/-}$ NK cells. Sorted splenic NK cells were expanded as in F, rested 4h, and stimulated 3h with IL-15/IL-15Rα complex (n=3 biological replicates per group).

H. Representative flow cytometry plots of splenic NK cell maturation in *Stat5a*$^{+/+}$ *Stat5b*$^{+/+}$ and *Stat5a*$^{-/-}$ *Stat5b*$^{+/-}$ mice. Data are representative of two independent experiments.

I. Fold change of *Id2* expression in splenic control (*Stat5a*$^{+/+}$ *Stat5b*$^{+/+}$) or *Stat5a*$^{-/-}$ *Stat5b*$^{+/-}$ NK cells (n=4 *Stat5a*$^{+/+}$ *Stat5b*$^{+/+}$ and 5 *Stat5a*$^{-/-}$ *Stat5b*$^{+/-}$ mice pooled from two independent experiments). Normalized to *Hprt* expression and shown as fold change relative to controls.

J. STAT5 occupancy at the *Id2* promoter. Splenic NK cells were sorted and expanded *in vitro* for 7d. Cells were rested for 2h in unsupplemented media, then stimulated with 20ng/mL IL-15/IL-15Rα complex for 1h. Fixed nuclei were then isolated for chromatin immunoprecipitation and qPCR (n=3 biological replicates per group).

*p≤0.05, **p≤0.01, ***p≤0.001. Two-tailed t-test; F and G were analyzed by one way ANOVA with Tukey's post hoc test. All error bars represent SEM. See also Figure S5.

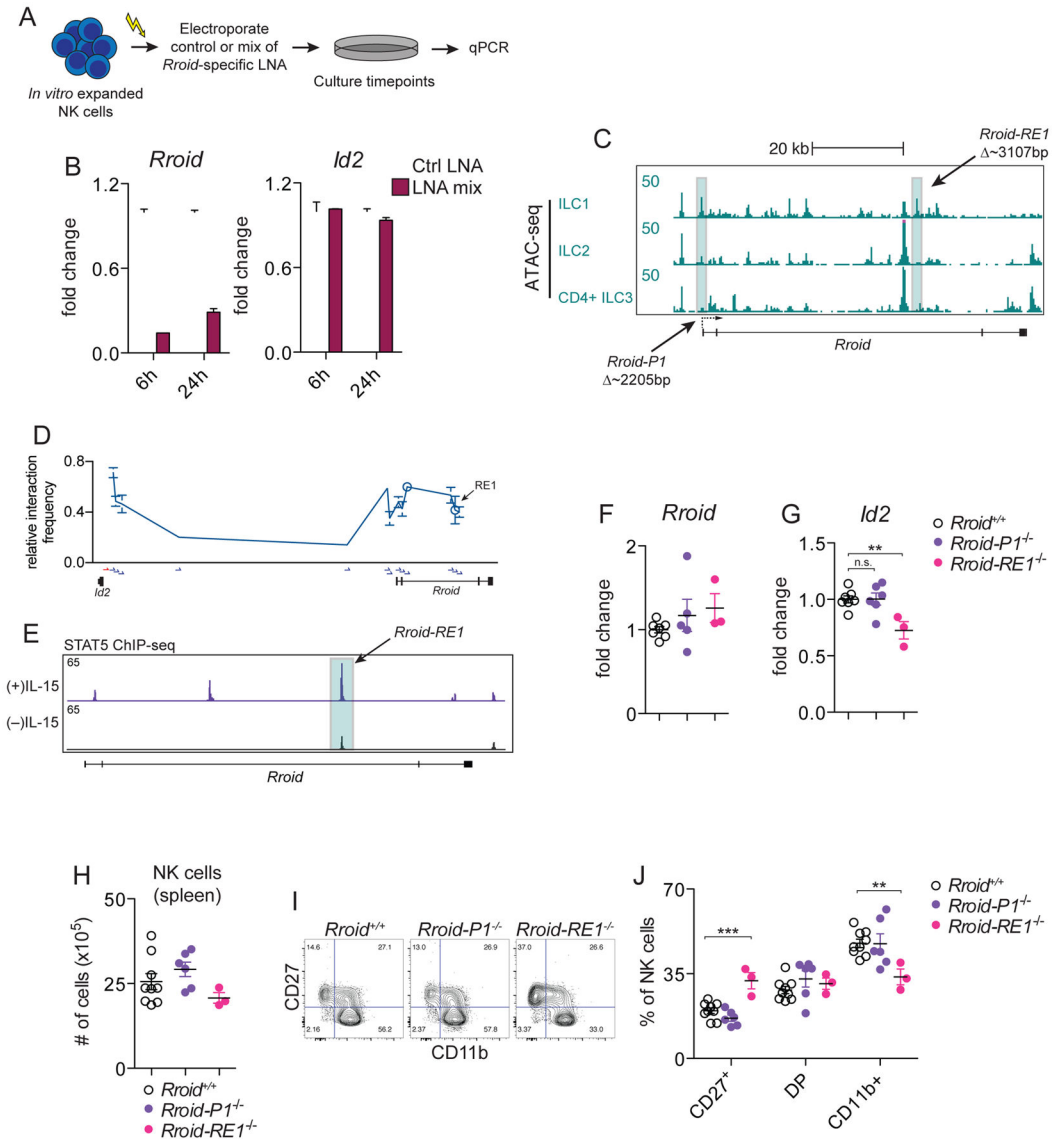

Figure 6. Deletion of *Rroid-E1* results in decreased mature NK cells and *Id2* expression

A. Schematic of locked nucleic acid (LNA) experiment. Sorted wild-type splenic NK cells were expanded *ex vivo* for 7d and electroporated with either 4μM control LNA or a 4μM mix of four LNAs targeting the *Rroid* RNA and cultured for either 6h or 24h.

B. qPCR analysis of *Rroid* (left) and *Id2* (right) expression at the indicated time points following electroporation with LNAs (n=2 biological replicates). Data are representative of two independent experiments. Normalized to *Hprt* expression and shown as fold change relative to controls.

C. Gene browser ATAC-seq tracks showing open chromatin within the *Rroid* locus. Highlighted are open chromatin peaks and CRISPR/Cas9-targeted regions for the *Rroid-P1* and *Rroid-RE1* knockouts.

D. Chromatin conformation capture (3C) of interactions between the *Id2* promoter and the indicated genomic regions. Data are normalized to interaction frequency of ligated BAC

templates containing the regions of interest. Primer locations are indicated by arrows; the bait primer located in the *Id2* promoter is indicated by the red arrow. (*n*=3 biological replicates). Data represent two independent experiments.

E. Gene browser view of STAT5 ChIP-seq showing binding at the *Rroid* locus in the presence or absence of IL-15 stimulation for 2h at 20ng/mL.

F. Fold change in *Rroid* expression in splenic NK cells sorted from 6–8 week old *Rroid-P1*$^{-/-}$, *Rroid-RE1*$^{-/-}$, and *Rroid*$^{+/+}$ littermate control mice as measured by qPCR (*n*=7 littermate controls (*Rroid*$^{+/+}$), 6 *Rroid-P1*$^{-/-}$, and 3 *Rroid-RE1*$^{-/-}$ mice per group). Normalized to *Hprt* expression and shown as fold change relative to littermate controls.

G. Fold change in *Id2* expression in splenic NK cells sorted from 6–8 week old *Rroid-P1*$^{-/-}$, *Rroid-RE1*$^{-/-}$, and *Rroid*$^{+/+}$ littermate control mice as measured by qPCR (*n*=7 littermate controls (*Rroid*$^{+/+}$), 6 *Rroid-P1*$^{-/-}$, and 3 *Rroid-RE1*$^{-/-}$ mice per group). Normalized to *Hprt* expression and shown as fold change relative to littermate controls.

H. Absolute numbers of splenic NK cells in 6–8 week old *Rroid-P1*$^{-/-}$, *Rroid-RE1*$^{-/-}$, and *Rroid*$^{+/+}$ littermate control mice (*n*=9 *Rroid*$^{+/+}$, 6 *Rroid-P1*$^{-/-}$, and 3 *Rroid-RE1*$^{-/-}$ mice per group).

I. Representative flow cytometry plots showing splenic NK cell maturation in in 6–8 week old *Rroid-P1*$^{-/-}$, *Rroid-RE1*$^{-/-}$, and *Rroid*$^{+/+}$ littermate control mice. Gated on live, CD45.2^{+} CD3, CD5, CD19^{-} NK1.1^{+} NKp46^{+} cells.

J. Frequency of maturing NK cell subsets. Splenic NK cells from 6–8 week old *Rroid-P1*$^{-/-}$, *Rroid-RE1*$^{-/-}$, and *Rroid*$^{+/+}$ littermate control mice were gated on live, CD45.2^{+} CD3, CD5, CD19^{-} NK1.1^{+} NKp46^{+} cells and analyzed for maturation markers (*n*=9 littermate controls (*Rroid*$^{+/+}$), 6 *Rroid-P1*$^{-/-}$, and 3 *Rroid-E1*$^{-/-}$ mice per group).

$*p \leq 0.05$, $**p \leq 0.01$, $***p \leq 0.001$. Two-tailed *t*-test. All error bars represent SEM. See also Figure S6.

KEY RESOURCES TABLE

REAGENT or RESOURCE	SOURCE	IDENTIFIER
Antibodies		
Anti-mouse CD3 (clone: 145-2C11)	ThermoFisher Scientific	47-0031-82
Anti-mouse CD4 (GK1.5)	Biolegend	100406
Anti-mouse CD8 (53-6.7)	Biolegend	100706
Anti-mouse/human CD11b (M1/70)	Biolegend	101212
Anti-mouse CD11c (N418)	Biolegend	117317
Anti-mouse CD19 (1D3)	ThermoFisher Scientific	47-0193-82
Anti-mouse CD25 (3C7)	Biolegend	101915
Anti-mouse/rat/human CD27 (LG.3A10)	Biolegend	124216
Anti-mouse CD28 (37.51)		
Anti-mouse CD45.1 (A20)	Biolegend	48-0453-82
Anti-mouse CD45.2 (104)	Biolegend	109822
Anti-mouse CD49a (HMα1)	Biolegend	142604
Anti-mouse CD49b (DX5)	Biolegend	108910
Anti-mouse CD90.2 (30-H12)	Biolegend	105324
Anti-mouse CD107a (1D4B)	Biolegend	121612
Anti-mouse/pig CD117 (2B8)	ThermoFisher Scientific	47-1171-80
Anti-mouse CD122 (TM-β1)	Biolegend	123213
Anti-mouse CD127 (A7R34)	Biolegend	135010
Anti-mouse 2B4 (m2B4(B6)458.1)	Biolegend	133508
Anti-mouse α4β7 Integrin (DATK32)	Biolegend	120612
Anti-BrdU (Bu20a)	Biolegend	339812
Anti-mouse Eomes (Dan11mag)	ThermoFisher Scientific	50-4875-82
Anti-mouse F4/80 (BM8)	Biolegend	123113
Anti-mouse Flt3 (A2F10)	Biolegend	135314
Anti-mouse GATA3 (L50-823)	BD Biosciences	135314
Anti-mouse IFN-γ (XMG1.2)	Biolegend	505826
Anti-mouse IL-2 (S4B6)	BioXcell	BE0043-1-5MG
Anti-mouse IL-4 (11B11)	Biolegend	504107
Anti-mouse IL-5 (TRFK5)	ThermoFisher Scientific	12-7052-81
Anti-mouse IL-13 (eBio13A)	ThermoFisher Scientific	53-7133-80
Anti-mouse IL-22 (IL22JOP)	ThermoFisher Scientific	17-7222-82
Anti-mouse Ly6G (1A8)	Biolegend	127606
Anti-mouse MHC-II (M5/114.15.2)	Biolegend	107621
Anti-mouse NK1.1 (PK136)	Biolegend	108745
Anti-mouse NKp46 (29A1.4)	Biolegend	137606
Anti-mouse Rorγt (B2D)	ThermoFisher	12-6981-82
	Scientific	

REAGENT or RESOURCE	SOURCE	IDENTIFIER
Anti-mouse Sca-1 (D7)	Biolegend	108131
Anti-mouse Siglec-F (E50-2440)	BD Biosciences	552126
Anti-mouse p-STAT4 (38/pSTAT4)	BD Biosciences	558137
Anti-mouse/human STAT5A/B (Rabbit polyclonal IgG)	R&D Systems	AF2168
Anti-mouse p-STAT5 (47/Stat5(pY694))	BD Biosciences	612567
Anti-mouse T1/ST2 (Biotin; DJ8)	MD Bioproducts	101001B
Anti-mouse/human T-bet (4B10)	Biolegend	644824
Anti-mouse TCRβ (H57-597)	Biolegend	109212
Anti-mouse Ter119 (TER-119)	Biolegend	116206
Anti-H3K27ac (Rabbit polyclonal)	Abcam	ab4729
Anti-H3K36me3 (Rabbit polyclonal)	Abcam	ab9050
Streptavidin	Biolegend	405207
7-AAD	Sigma	A9400-1MG
DAPI	Sigma	D9542-5MG
Live/Dead Aqua	ThermoFisher Scientific	L34966
Bacterial and Virus Strains		
Listeria monocytogenes 1043S	Laboratory of E. John Wherry	N/A
Samonella enterica serovar Typhimurium (SL1344)	Laboratory of Igor Brodsky	N/A
Biological Samples		
Chemicals, Peptides, and Recombinant Proteins		
BrdU	Sigma	B5002-1G
Papain	Millipore	5125-50GM
Liberase TM	Sigma	5401127001
Collagenase D	Sigma	11088866001
Collagenase 4	Worthington Biochemical	LS004188
DNase I	Sigma	DN25-1G
Percoll	GE Healthcare	17-0891-01
Recombinant human IL-2	Peprotech	200-02
Recombinant mouse IL-2	Peprotech	212-12
Recombinant mouse IL-3	Biolegend	575502
Recombinant mouse IL-6	Biolegend	575702
Recombinant mouse IL-12	Biolegend	577002
Recombinant mouse IL-15/IL-15Rα	ThermoFisher Scientific	14-8152-80
Recombinant mouse IL-18	MBL International	B002-5
Recombinant mouse IL-23	ThermoFisher Scientific	14-8231-63
Recombinant mouse IL-33	Biolegend	580504
Recombinant mouse SCF	Biolegend	579702
Critical Commercial Assays		
KAPA SYRBR Fast	KAPA Biosystems	KK4618

REAGENT or RESOURCE	SOURCE	IDENTIFIER
Cells-to-CT 1-Step TaqMan Kit	ThermoFisher Scientific	A25605
Protein G Dynabeads	ThermoFisher Scientific	10004D
BioMag Goat Anti-Rat IgG	Qiagen	310107
Foxp3 Transcription Factor Staining Kit	ThermoFisher Scientific	00-5523-00
Cytofix/Cytoperm	BD Biosciences	554722
Permeabilization buffer	ThermoFisher Scientific	00-8333-56
BrdU staining buffer set	ThermoFisher Scientific	00-5525-00
Deposited Data		
Raw RNA-seq and ATAC-seq data	This paper	GEO: GSE101459
ILC RNA-seq and ATAC-seq tracks	(Shih et al., 2016)	GEO: GSE77695
RNA-seq from *Id2*-deficient NK cells	(Delconte et al., 2016)	GEO: GSE76466
STAT5 ChIP-seq tracks from NK cells	(Villarino et al., 2017, In Press)	GEO: GSE100674
Experimental Models: Cell Lines		
RMA	Laboratory of Taku Kambayashi	N/A
RMA-S	Laboratory of Taku Kambayashi	N/A
Experimental Models: Organisms/Strains		
Mouse: *Rroid*$^{-/-}$	This paper	N/A
Mouse: *Rroid-P1*$^{-/-}$	This paper	N/A
Mouse: *Rroid-E1*$^{-/-}$	This paper	N/A
Mouse: C57BL/6	Jackson Laboratory	JAX: 00664
Mouse: B6.SJL-*Ptprc*^{a} *Pepc*^{b}/Boy (CD45.1^{+})	Jackson Laboratory	JAX: 002014
Mouse: *Zbtb16*$^{tm1.1(EGFP/cre)Aben}$ (PLZF^{GFPcre})	Jackson Laboratory	JAX: 024529
Mouse: *Stat5a*$^{-/-}$ *Stat5b*$^{+/-}$	Laboratory of John J. O'Shea	N/A
Mouse: *Tbx21*$^{-/-}$	Laboratory of Christopher Hunter	N/A
Oligonucleotides		
Primers for PCR and qPCR located in Table S2		
Rroid-5′ sgRNA: GATTCACAGGCACTTGTTTCG TTTTAGAGCTAGAAATAGCAAGTTAAA ATAAGGCTAGTCCGTTATCAACTTGA AAAAGTGGCACCGAGTCGGTGCTTTTTT	This paper	N/A
Rroid-3′ sgRNA: GCTATAGGTGTTAATTCTGTG TTTTAGAGCTAGAAATAGCAAGTTAAA ATAAGGCTAGTCCGTTATCAACTTGA AAAAGTGGCACCGAGTCGGTGCTTTTTT	This paper	N/A
Rroid-P1-5′ sgRNA: GTATGATAAACTCACAATGG GTTTTAGAGCTAGAAATAGCAAGTTAAAA TAAGGCTAGTCCGTTATCAACTTGA AAAAGTGGCACCGAGTCGGTGCTTTTTT	This paper	N/A
Rroid-P1-3′ sgRNA:	This paper	N/A
TCGCTTCAGAGGGCACTATAGTTTTA GAGCTAGAAA		
TAGCAAGTTAAAATAAGGCTAGTCCG TTATCAACTT		
GAAAAAGTGGCACCGAGTCGGTGCTTTTTT		

REAGENT or RESOURCE	SOURCE	IDENTIFIER
Rroid-RE1-5´ sgRNA: TGTCCAAGGATGTCCATATT GTTTTAGAGCTAGAAATAGCAAGTTAAAAT AAGGCTAGTCCGTTATCAACTTGAA AAAGTGGCACCGAGTCGGTGCTTTTTT	This paper	N/A
Rroid-RE1-3´ sgRNA: CATCCGAAGATCCCTGTATG GTTTTAGAGCTAGAAATAGCAAGTTAAAA TAAGGCTAGTCCGTTATCAACTTGAA AAAGTGGCACCGAGTCGGTGCTTTTTT	This paper	N/A
Recombinant DNA		
RP23-300A18	Bacpac	N/A
RP23-342B16	Bacpac	N/A
Software and Algorithms		
FlowJo v10.3	Tree Star	https://www.flowjo.com/solutions/flowjo
Graphpad Prism 7	GraphPad Software	https://www.graphpad.com/
Fiji	(Schindelin et al., 2012)	https://fiji.sc/
Other		